catalysts

MDPI

Review

Eco-Friendly Colloidal Aqueous Sol-Gel Process for TiO_2 Synthesis: The Peptization Method to Obtain Crystalline and Photoactive Materials at Low Temperature

Julien G. Mahy [1,*], Louise Lejeune [1], Tommy Haynes [1], Stéphanie D. Lambert [2], Raphael Henrique Marques Marcilli [3], Charles-André Fustin [3] and Sophie Hermans [1,*]

[1] Molecular Chemistry, Materials and Catalysis (MOST), Institute of Condensed Matter and Nanosciences (IMCN), Université Catholique de Louvain, Place Louis Pasteur 1, B-1348 Louvain-la-Neuve, Belgium; l.lejeune@student.uclouvain.be (L.L.); tommy.haynes@uclouvain.be (T.H.)

[2] Department of Chemical Engineering—Nanomaterials, Catalysis, Electrochemistry, B6a, University of Liège, B-4000 Liège, Belgium; stephanie.lambert@uliege.be

[3] Bio and Soft Matter Division (BSMA), Institute of Condensed Matter and Nanosciences (IMCN), Université Catholique de Louvain, Place Louis Pasteur 1, B-1348 Louvain-la-Neuve, Belgium; raphael.marques@uclouvain.be (R.H.M.M.); charles-andre.fustin@uclouvain.be (C.-A.F.)

* Correspondence: julien.mahy@uclouvain.be (J.G.M.); sophie.hermans@uclouvain.be (S.H.); Tel.: +32-10-47-28-10 (S.H.)

Abstract: This work reviews an eco-friendly process for producing TiO_2 via colloidal aqueous sol–gel synthesis, resulting in crystalline materials without a calcination step. Three types of colloidal aqueous TiO_2 are reviewed: the as-synthesized type obtained directly after synthesis, without any specific treatment; the calcined, obtained after a subsequent calcination step; and the hydrothermal, obtained after a specific autoclave treatment. This eco-friendly process is based on the hydrolysis of a Ti precursor in excess of water, followed by the peptization of the precipitated TiO_2. Compared to classical TiO_2 synthesis, this method results in crystalline TiO_2 nanoparticles without any thermal treatment and uses only small amounts of organic chemicals. Depending on the synthesis parameters, the three crystalline phases of TiO_2 (anatase, brookite, and rutile) can be obtained. The morphology of the nanoparticles can also be tailored by the synthesis parameters. The most important parameter is the peptizing agent. Indeed, depending on its acidic or basic character and also on its amount, it can modulate the crystallinity and morphology of TiO_2. Colloidal aqueous TiO_2 photocatalysts are mainly being used in various photocatalytic reactions for organic pollutant degradation. The as-synthesized materials seem to have equivalent photocatalytic efficiency to the photocatalysts post-treated with thermal treatments and the commercial Evonik Aeroxide P25, which is produced by a high-temperature process. Indeed, as-prepared, the TiO_2 photocatalysts present a high specific surface area and crystalline phases. Emerging applications are also referenced, such as elaborating catalysts for fuel cells, nanocomposite drug delivery systems, or the inkjet printing of microstructures. Only a few works have explored these new properties, giving a lot of potential avenues for studying this eco-friendly TiO_2 synthesis method for innovative implementations.

Keywords: TiO_2; photocatalysis; sol–gel synthesis; peptization; doping; pollutant degradation; mild temperature

Citation: Mahy, J.G.; Lejeune, L.; Haynes, T.; Lambert, S.D.; Marcilli, R.H.M.; Fustin, C.-A.; Hermans, S. Eco-Friendly Colloidal Aqueous Sol-Gel Process for TiO_2 Synthesis: The Peptization Method to Obtain Crystalline and Photoactive Materials at Low Temperature. *Catalysts* **2021**, *11*, 768. https://doi.org/10.3390/catal11070768

Academic Editor: Ewa Kowalska

Received: 4 June 2021
Accepted: 21 June 2021
Published: 24 June 2021

1. Introduction

Photocatalysis is a well-established process for the effective and sustainable removal of a large range of organic pollutants, both in liquid and gaseous media [1]. This phenomenon consists of a set of oxidation-reduction (redox) reactions between the organic compounds (pollutants) and the active species formed at the surface of an illuminated photo-

catalyst (usually a photoactivable semiconductor solid). Generally, when the solid photocatalyst is illuminated (Figure 1), electrons from the valence band are promoted to the conduction band. This results in electron–hole pairs, which can react with O_2 and H_2O, adsorbed at the surface of the photocatalyst, to produce hydroxyl (•OH) and superoxide ($O_2^{-\bullet}$) radicals. These radicals can attack organic molecules and induce their degradation in CO_2 and H_2O, if the degradation is complete [2].

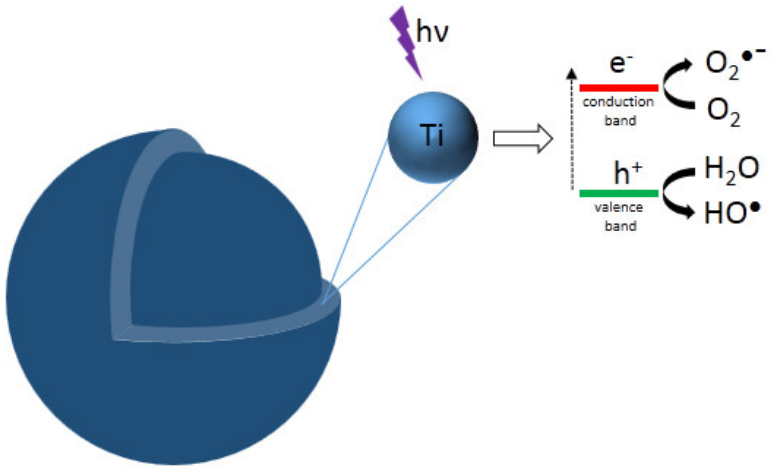

Figure 1. Schematic representation of photocatalytic TiO_2 NP: photogenerated charges (electron and hole) upon absorption of radiation.

Various semi-conductors can be used as photocatalysts, such as NiO [3], ZnO [4], CeO_2 [5], MnO_2 [6], or TiO_2 [7]. The most widely used solid photocatalyst is TiO_2 [7,8], which is a non-toxic and cheap semiconductor sensitive to UV radiation [8]. TiO_2 exists in three different crystallographic structures: anatase (tetragonal structure with a band gap of 3.2 eV), brookite (orthorhombic structure with a band gap >3.2 eV), and rutile (tetragonal structure with a band gap of 3.0 eV) [7]. The best phase for photocatalytic applications is anatase [7]. However, the use of TiO_2 as a photocatalyst has two main limitations [7]: (i) the fast charge recombination, and (ii) the high band gap value which calls for UV light for activation. Therefore, the amount of energy required to activate anatase TiO_2 is high. Indeed, its band gap width (3.2 eV) corresponds to light with a wavelength inferior or equal to 388 nm [7] and so, in the case of illumination by natural light, only the most energetic light will be used for activation, which corresponds to 5–8% of the solar spectrum [8]. To prevent these limitations, several studies have been conducted [9–12] to increase the recombination time and extend the activity towards the visible range. Most works consisted in modifying TiO_2 materials by doping or modification with a large range of different elements, such as Ag [9], P [13], N [14], Fe [11,12], porphyrin [15,16], etc. Therefore, the synthesis process of TiO_2 must be easily adjustable to incorporate such dopants/additives when needed, depending on the targeted application.

Several processes exist to produce TiO_2 photocatalysts, the main methods being chemical or physical vapor deposition [17,18], aerosol process [19], microwave [20], reverse micelle [21], hydrothermal [22], and laser pyrolysis [23]. These processes often use severe synthesis conditions, such as high pressure, high-temperature, or complex protocols. Another possible synthesis pathway is the sol–gel method [24], which has proven to be effective for the synthesis of TiO_2 in the form of powders or films, with control of the nanostructure and surface properties [25–29]. The sol–gel process is classified among "soft

chemistry" protocols because reactions occur at low temperature and low pressure. The titanium precursor, usually an alkoxide, undergoes two main reactions: hydrolysis and condensation ((1)–(3) from Figure 2) [24,30,31]. The condensation gives the Ti-O-Ti network formation.

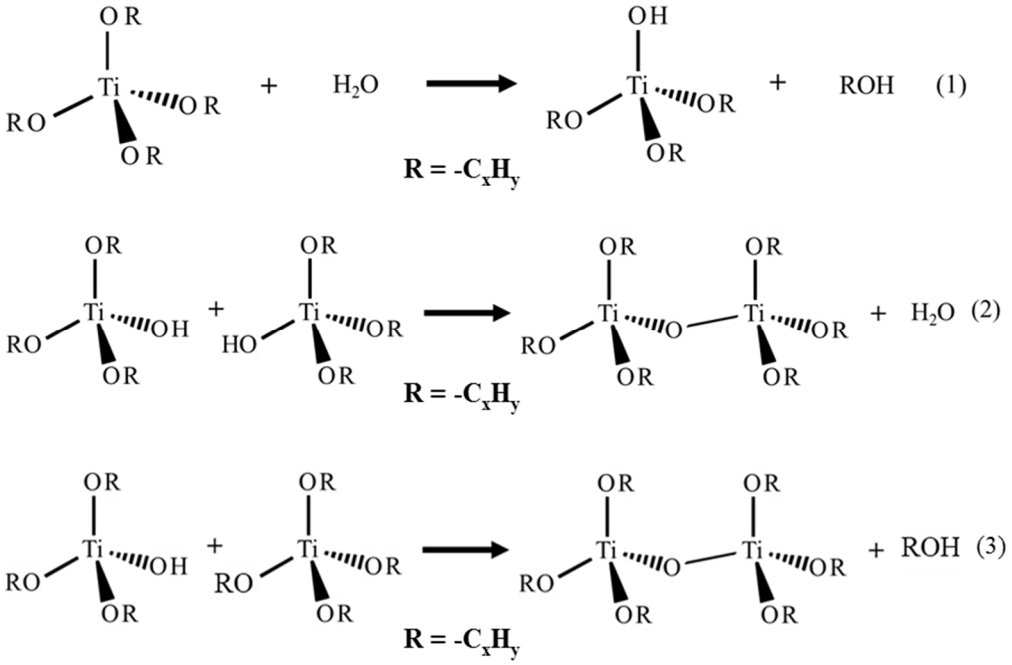

Figure 2. Hydrolysis and condensation reactions of the sol–gel process with Ti alkoxide precursor.

By controlling the rate of the hydrolysis and condensation reactions, a liquid sol or a solid gel is obtained. In order to produce TiO_2 by sol–gel processes, an organic solvent is often used. This organic solvent, such as 2-methoxyethanol, is able to complex the titanium precursor (for example, titanium tetraisopropoxide, TTIP, Ti-$(OC_3H7)_4$) to control its reactivity. A stoichiometric amount of water is added to avoid fast precipitation [24,31]. The material then undergoes drying and calcination steps to remove residual organic molecules and to crystallize amorphous TiO_2 in anatase, brookite, or rutile phases [32]. In the last decade, attempts at reducing the use of large amounts of organic solvent have been heavily investigated, in order to develop greener syntheses. The use of water as the main solvent was made possible by the use of a peptizing agent. By definition, a peptizing agent (PA) is a substance that, even in small amounts, prevents the agglomeration/flocculation of particles and a decrease in viscosity through enhancing the dispersion in aqueous media [33]. The PA allows crystallization at low temperature, even if the titanium precursor has precipitated. The synthesis of high crystalline TiO_2 nanoparticles, through colloidal aqueous sol–gel in presence of PA, has been successfully reported in the literature [34] and is the main subject of this review.

This synthesis path was first referenced at the end of the 1980s [35–37]. Water is present in a large excess compared to the Ti precursor, and peptizing agents are used to form small TiO_2-crystalline nanoparticles from various Ti precursors at low temperature (<100 °C) [8,38,39], resulting in the formation of a crystalline colloid. Although it is seldom used in the development of TiO_2 synthesis processes, since organic solvents are preferred to better control the Ti precursor reactivity, this preparation method presents a lot of advantages and fulfills the principles of green chemistry that are currently being promoted: (i) the synthesis conditions are soft as it is a sol–gel process; (ii) easy protocol with no risky conditions; (iii) low use of organic reagents, as water is the main solvent; and (iv) crystalline materials are obtained without thermal treatment. Additionally, this synthesis has other advantages, such as: (i) very stable colloids are obtained, allowing the elaboration

of coatings very easily by classical deposition techniques (spray-, dip-, spin-, or bar-coating); (ii) protocol easily modified to introduce dopants or additives; and (iii) production at larger scale, up to 20 L.

The goal of this review is to evaluate the state of the art of the research into this not very well-known eco-friendly process for producing TiO_2 via colloidal aqueous sol–gel synthesis, resulting in crystalline materials without a calcination step. A literature review allowed us to find about 115 articles making use of this synthesis process to produce TiO_2 materials, spanning from 1987 to 2020. Figure 3 represents the year distribution of these 115 articles. The number of articles over the past 30 years was quite low, due to several reasons: (i) the hydrolysis of the Ti precursor is much easier to control in alcohol solvent and (ii) very fast in water, (iii) the use of water to replace organic solvents for greener processes is a quite recent requirement in chemical processes. Nevertheless, the development of this process has become more and more important over the last ten years.

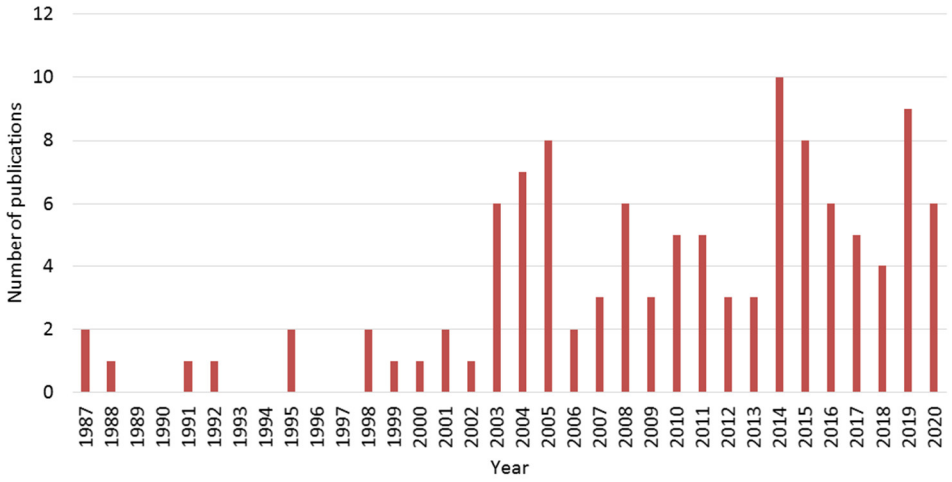

Figure 3. Number of publications per year about colloidal aqueous sol–gel synthesis of TiO_2 materials collected for this review.

An increase of interest in this topic in the past ten years is clearly observed. Throughout this review article, the synthesis protocol will be detailed with a focus on the most important parameters, in order to template the resulting TiO_2 material. Indeed, by changing synthesis parameters, the three different phases of TiO_2 can be obtained, without any thermal treatments. Moreover, specific morphologies can also be produced. In some of the selected articles, thermal post-treatments (calcination or hydrothermal treatment) are applied to the as-synthesized materials, therefore their impact on the crystallinity and morphology of the resulting TiO_2 materials will also be reviewed in this paper.

Finally, the photocatalytic properties of these aqueous TiO_2 materials will be also reviewed and linked to their physico-chemical characteristics. In the end, new emerging applications will be highlighted.

2. Synthesis of TiO_2 with PA in Water

The synthesis uses three main components: the Ti precursor, the peptizing agent, and water. Two operations will take place during the synthesis: the precipitation and the peptization. Indeed, usually the Ti precursor is very reactive on contact with water, resulting in its rapid hydrolysis and condensation. It produces a precipitate of mainly amorphous TiO_2. Then, the addition of the peptizing agent will induce the peptization, i.e., the slow dissolution of the TiO_2 precipitate and its crystallization into small TiO_2 crystallites (<10 nm). Indeed, the introduction of peptizing agent modifies the pH of the solution and increases the solubility of the amorphous titania [39]. The heating of the solution further increases the dissolution of this amorphous TiO_2 and accelerates the crystallization [40].

The high concentration of hydroxylated titanium leads to a rapid crystallization, with high nucleation rate [40]. Due to this rapid nucleation rate, metastable polymorphs (i.e., anatase and brookite phases) are favored. When the crystallization is slower, the stable rutile phase is produced [39,40].

Figure 4 presents the general scheme of the synthesis. Usually, the reaction medium can be heated up to 95 °C during peptization.

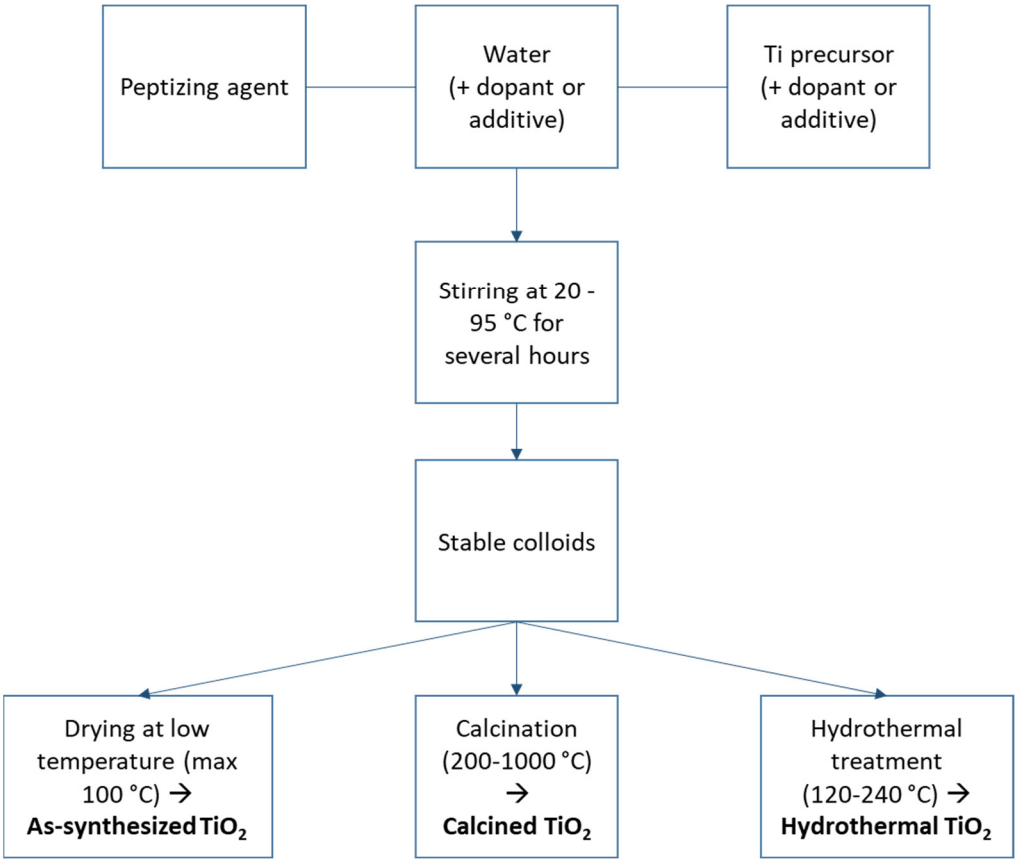

Figure 4. General scheme of the sol–gel TiO_2 colloidal aqueous synthesis.

The resulting colloids are very stable (up to years [41]) due to the surface charges of the nanoparticles and can be composed of different crystalline phases and morphologies, depending on the synthesis parameters. The parameters that can be varied are: the type and amount of peptizing agent, the temperature and duration of peptization, and the type of Ti precursor.

Numerous variants of these synthetic parameters have been collected and summarized in Table 1. In addition to the above-mentioned components, possible dopants, applied post-treatments, and shapings are also listed. From this summary, it appears clear that the most used Ti precursor is titanium isopropoxide (TTIP), used in 75 out of the 115 considered studies, due to its relatively low cost; while the peptizing agent is mainly nitric acid (in 71 out of 115 works). The reaction mixture is often heated to reduce the reaction time. When doping is performed, mainly metallic or nitrogen species are used, as they are the main dopants that are known to enhance TiO_2 photoactivity. Each author tries to keep the synthesis protocol easy and eco-friendly by reducing the amount of additive/dopant used during the synthesis process. Some organic solvents can be added to stabilize the Ti precursor during the synthesis, but only in very small quantities (less than 10% in volume). With the obtained colloids, it is easy to produce materials with different shapes, such as coatings on various substrates, powders by just drying the colloids, or as colloids directly. The study of Douven et al. [42] refers to the possibility of easily synthesizing

colloidal aqueous TiO_2 at larger scale, up to 10 L batches. This shows the potential for scaling-up towards industrial scale.

Table 1. Main TiO_2 synthesis parameters.

Synthesis Parameters	Corresponding Parameters Collected in the Literature (Variants)
Ti precursor	Ti isopropoxide [8,16,34,35,38,41–95], Ti ethoxide [39,96], Ti butoxide [37,97–103], Ti trichloride [104,105], Ti tetrachloride [106–113], Titanyl sulfate and disulfate [114–117], Titanium(IV) bis(acetylacetonate) diisopropoxide [118], metatitanic acid [119–122], Ti propoxide [96].
Peptizing agent	Nitric acid [8,16,36,39,41–43,45,46,53,56,59,61,62,64,66,67,70,73,76–79,82,86,93,96,100,106,107,109,114,117,119,120,123–131], acetic acid [37,44,87,125,132,133], hydrochloric acid [39,49,54,68,72,87,104,108,121,134–139], malonic acid [125], sulfuric acid [39,53,89,107], tetramethylammonium hydroxide [50,101,140], sodium hydroxide [52,54], phosphoric acid [54,107], perchloric acid [83,141], ammonium hydroxide [38,58,91], hydrogen peroxide [105,116], lactic acid [71], citric acid [138], boric acid [85]
Temperature range of reaction	20–95 °C
Trace of organic solvent	Isopropanol, ethanol, methanol
Additive or dopant	Other metallic alkoxides, metallic salts, carbon materials, nitrogen compounds
Thermal treatment	Ambient drying, calcination in the range 200–1000 °C, hydrothermal treatment
Shaping	Powder, coating, colloid

3. Crystallinity

One of the main advantages of this colloidal aqueous TiO_2 synthesis method is to produce crystalline materials without any thermal treatment. Nevertheless, some studies performed post-synthetic hydrothermal and/or calcination steps in order to obtain specific physico-chemical properties. The following sections detail the crystalline properties obtained depending on these three possibilities: as-synthesized, after calcination, or hydrothermal treatments.

3.1. As-Synthesized Aqueous TiO_2

As mentioned, after the synthesis, a stable TiO_2 colloid in water is obtained. This suspension can be dried under ambient air or precipitated by a pH change to recover the as-synthesized powder. This powder can be easily redispersed in acidic water [41]. In the majority of the reviewed studies, the powders are characterized by XRD in order to evaluate their crystalline phases.

Concerning the crystallinity, the peptizing agent seems to play a very important role. Indeed, the three different TiO_2 phases, namely anatase/brookite/rutile, can be obtained by merely changing the amount of peptizing agent, its acid-basic character, or the nature of the counter ion [82]. In all these studies, the crystallite size remains in the same range, between 3 and 10 nm [47,78].

3.1.1. Acid Peptizing Agent

With the most used peptizing agent, HNO_3, when it is used without any other additive, a mixture of anatase/brookite is often produced, [39,76,87,97,142]; with a higher proportion of anatase, as presented in Figure 5a. Only the peak at 30.8° is observed for brookite. An increase in the amount of HNO_3 during peptization (from pH of 2 up to pH of 0.5) induces the formation of rutile phase, as show in [39,118,143]. A mixture of crystalline phases is often reported. When additives that cause a shift in pH value are used, the distribution can be modified. In the works of Burda et al. [133] and Chen et al. [95], only anatase is produced when amine is added with HNO_3 at the beginning of the synthesis.

With HCl, which is the second most common peptizing agent used, anatase or anatase/brookite is also mainly reported [39,69,121,135,138,139]. A mixture of anatase/rutile is also produced when the amount of HCl increases [104,107,139]. At very high concentration, such as a Ti/H^+ molar ratio of 0.08, rutile alone is even observed [108]. Moreover, when different types of acids are used in the same concentration, different phase distributions can be obtained. As examples, Vinogradov et al. [87] used a Ti/H^+ ratio of 0.5, and obtained anatase/brookite mixtures with HNO_3 or HCl, while only anatase was produced with acetic acid, and an anatase/Ti sulfate mixture with H_2SO_4. This suggests that the counter ion (Bronsted conjugate base) also plays an important role in the preferential crystalline phase formed [87]. In Kanna et al. [107], with a similar acid amount (not specified), anatase is produced with H_2SO_4 and H_3PO_4, and an anatase/rutile mixture with HNO_3, HCl, or acetic acid. With carboxylic acids such as acetic, lactic, malonic, or citric acid, anatase is the main phase reported [57,74,76,87,125,133,138], as shown in Figure 5b. Only Kanna et al. [107] report an anatase/rutile mixture.

Globally, when inorganic acid is used, anatase and/or brookite phases are produced, but when the amount of acid leads to a pH smaller than 1, rutile phase is also produced. With organic acids, only anatase phase is formed. The different distributions of phases will impact the resulting surface area. Indeed, anatase and brookite phases lead to a higher specific surface area than rutile [63].

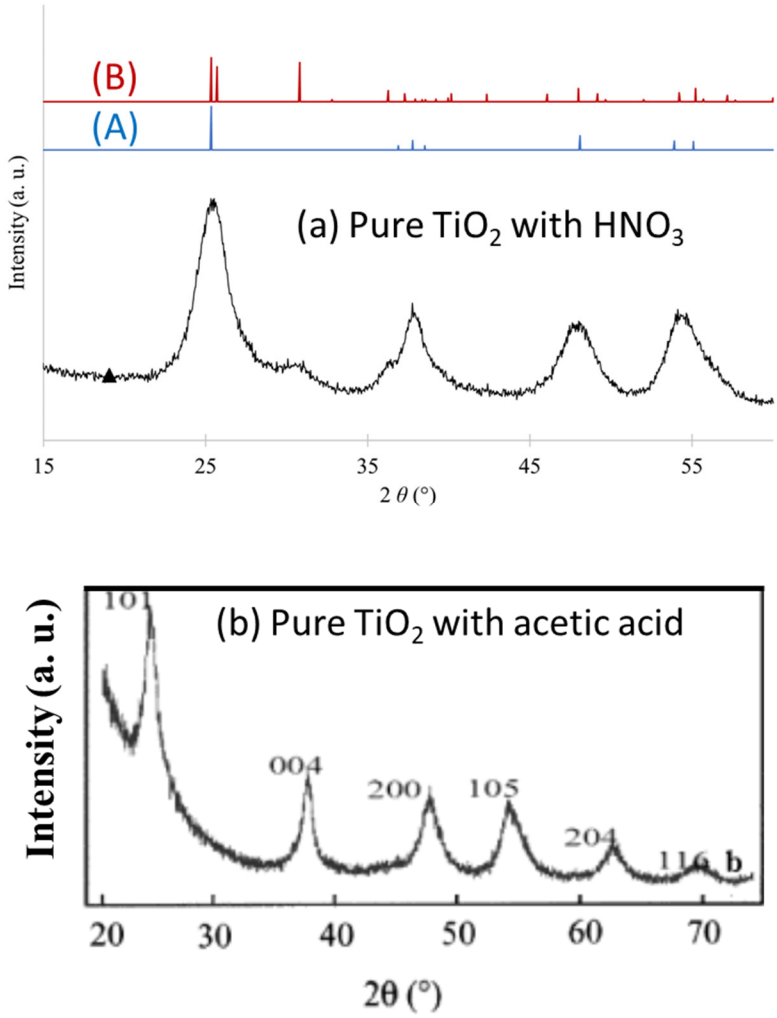

Figure 5. XRD patterns of pure TiO_2 material obtained with (**a**) HNO_3, where A stands for anatase phase and B for brookite phase from [142] (reproduced with permission from J. G. Mahy et al., AIMS Materials Science; published by AIMS Press, 2018, open access); and (**b**) acetic acid peptizing agents,

from [133] (reproduced with permission from J. L. Gole et al., The Journal of Physical Chemistry B; published by The American Chemical Society, 2004).

3.1.2. Basic Peptizing Agent

The basic peptization is far less common (about 8 out of 115 references considered in this review), but some studies still reference it. In Mashid et al. [38], NH_4OH is used to synthesize anatase/brookite mixture, as illustrated in Figure 6 for pH 8 and 9. Similarly, with NaOH anatase/brookite is reported in Mutuma et al. [70]. In Yu et al. [91], only anatase is observed with NH_4OH peptizing agent at high pH. Zhang et al. [113] report an anatase/rutile mixture with NH_4OH at neutral pH. To conclude, the nature (acidic or basic) of the peptizing agent and the amount used will impact the resulting phases, but the type of phase is difficult to predict.

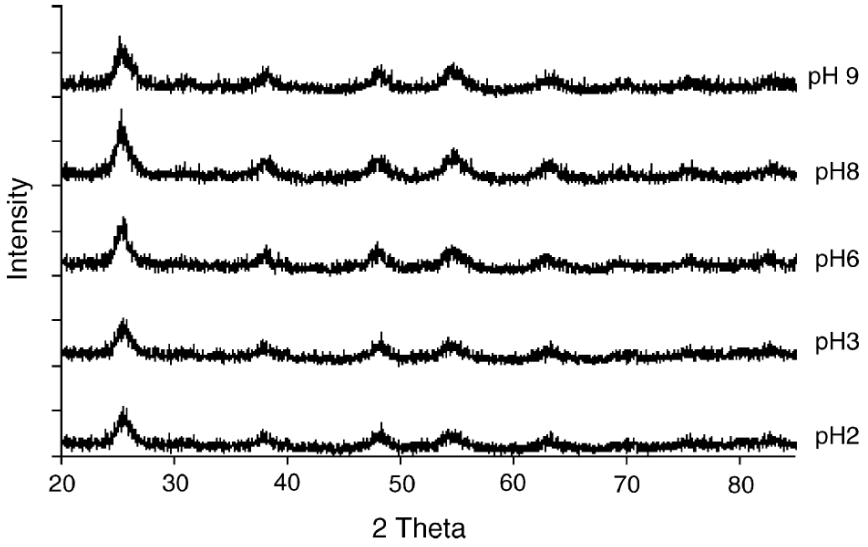

Figure 6. XRD patterns of pure TiO_2 obtained at different pH values, with HNO_3 (pH < 7) or NH_4OH (pH > 7) peptizing agent, from [38] (reproduced with permission from S. Mahshid et al., Journal of Materials Processing Technology; published by Elsevier, 2007).

As shown in the above paragraphs, both acidic or basic PA lead to crystalline TiO_2 materials. It is worth mentioning that the resulting TiO_2 materials are not 100% crystalline, as is the case when thermal treatments such as calcination or hydrothermal treatment (next paragraphs) are applied. Nevertheless, it was shown [63,65] that the crystalline fraction can be quite high (up to 85–90%) and that this fraction can be optimized by playing with the synthesis parameters, such as the time of reaction or the amount of PA.

3.2. Aqueous TiO_2 after a Calcination Treatment

Even if a crystalline material is already obtained right after the synthesis, often composed of two or three TiO_2 crystalline phases, as shown in the previous section, a large range of studies perform a calcination step to further crystallize the TiO_2 materials, also leading to an increase in the crystallite sizes. When the calcination temperature is high (>600 °C), rutile is often produced, as it is the most stable phase at high-temperature, as represented in Figure 7 [144]. Nie et al. [144] present a study of a structural dependence in function of the temperature and pressure on the calcination post-treatment of TiO_2, Figure 7. For temperatures below T <200 °C and pressure lower than 2 GPa the preferential crystalline phase is anatase, for calcinations in the same range of temperatures but with pressures higher than 2 GPa, the preferred crystalline phase formed is srilankite. On the other hand, for calcination performed at a temperature higher than 600 °C a preferential

rutile phase is normally observed, independent of the applied pressure, Figure 7. Additionally, a phase anatase–rutile transition is often observed around 500 °C.

The phase transition from brookite to anatase or rutile has been less studied and no phase diagram is found in the literature. Nevertheless, some authors claimed that brookite evolves to anatase then rutile when the calcination temperature increases, [145,146], while others claim than brookite evolves directly to rutile [147,148].

In the considered studies, the temperature of calcination varies between 200 and 1000 °C. In all of these cases, the crystallite size increases, from 3–10 nm in the as-synthesized TiO_2 materials, to a range of 20–100 nm, depending on the calcination temperature [45,46,86,149]. Obviously, the higher the temperature, the higher the obtained size.

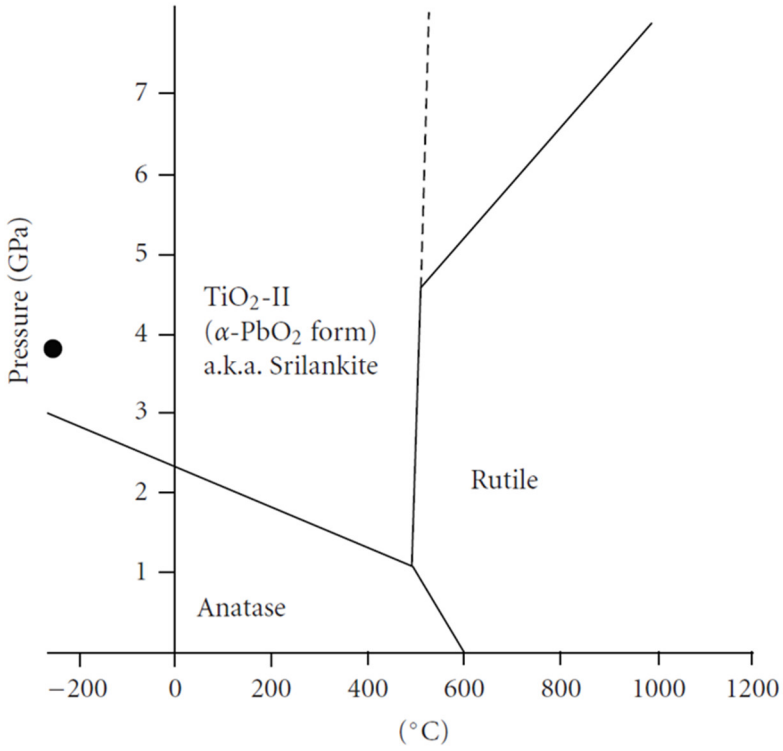

Figure 7. TiO_2 phase transition diagram from [144] (reproduced with permission from X. Nie et al., International Journal of Photoenergy; published by Hindawi Publishing Corporation, 2009, open access).

3.2.1. Calcination after Acidic Peptization

In Borlaf et al. [93], a HNO_3 peptized TiO_2 colloid is calcined between 200 and 1000 °C, and the crystalline phases are compared at various temperatures. As-synthesized, the TiO_2 material is composed of an anatase/brookite mixture, whose crystallite size increases, while keeping the same crystalline mixture until 500 °C. From 600 °C to 800 °C, the mixture is composed of anatase/rutile, with the proportion of rutile increasing with the temperature. From 800 to 1000 °C, only rutile is present. This is illustrated in Figure 8.

In [38,43,45,49,53,60,69,70,80,89,112,130,134], similar evolutions are obtained when using HNO_3 or HCl peptizer followed by a calcination from 300 to 900 °C. The anatase/brookite mixture is converted into a anatase/brookite/rutile mixture around 500 °C and becomes only rutile around 700 °C. Globally, the colloidal aqueous TiO_2 synthesis allows keeping anatase/brookite phase until 500–700 °C during calcination [58,71,73,85,91,98,114,129,130], which is coherent with the anatase-to-rutile transition temperature (Figure 7).

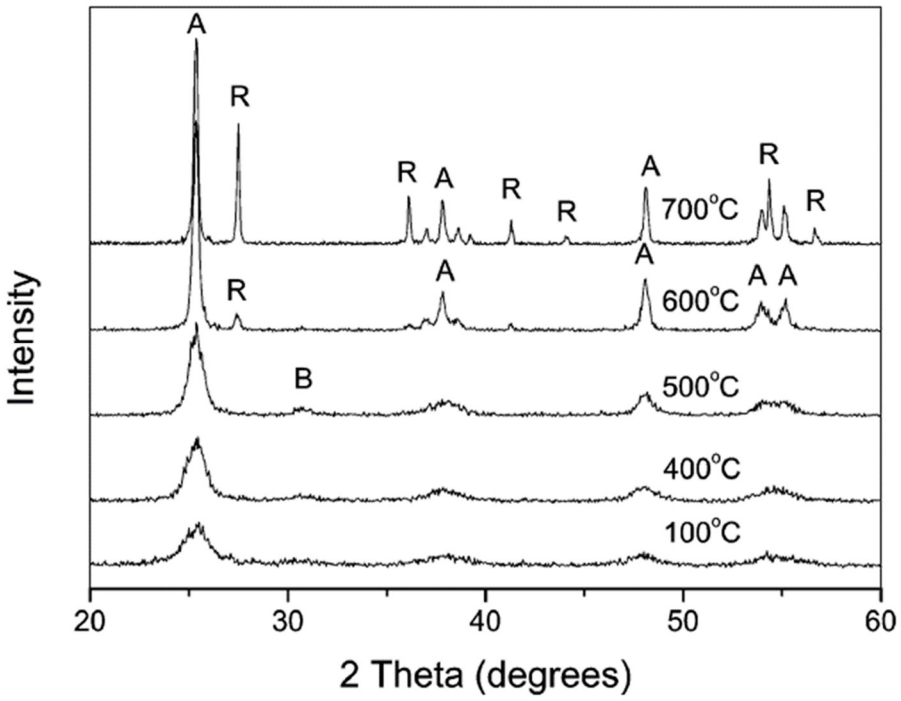

Figure 8. Evolution of the XRD pattern of a TiO_2 sample peptized with HNO_3 and calcined at different temperatures, from [91]. The A, B, and R labels stand for anatase, brookite, and rutile phases, respectively (reproduced with permission from J. Yu et al., Journal of Catalysis; published by Elsevier, 2003).

3.2.2. Basic Peptization Followed by Calcination

The same trends are globally observed in the case of the basic peptizers, even if these are less studied: an increase in anatase or anatase/brookite content is observed until a calcination temperature around 500–700 °C [52,58,70,91], then rutile becomes the main phase, as illustrated in Figure 9 [58,70,91].

3.3. Aqueous TiO_2 after Hydrothermal Treatment

This treatment consists in placing the precursor suspension in water in an autoclave under pressure, and heated at a controlled temperature. Similarly to calcination, a hydrothermal treatment allows the increase of the crystallinity of the as-synthesized samples thanks to the Ostwald ripening mechanism [50]. The temperature of such a treatment is usually between 170 and 240 °C. The crystallite size increases compared to the as-synthesized TiO_2 crystallite, in the range of 5 to 70 nm. When the treatment is very long (i.e., several days), a phase change may occur towards rutile (thermodynamically the most stable). A calcination step can be also applied after the hydrothermal treatment, and this will further increase the crystallite size of the phase present after the hydrothermal treatment [55,90,103,109,140,150], until the temperature of anatase-to-rutile transition is reached, where only rutile crystallites continue to grow [55,150]. For both types of peptizers, acid or basic, similar evolutions are observed.

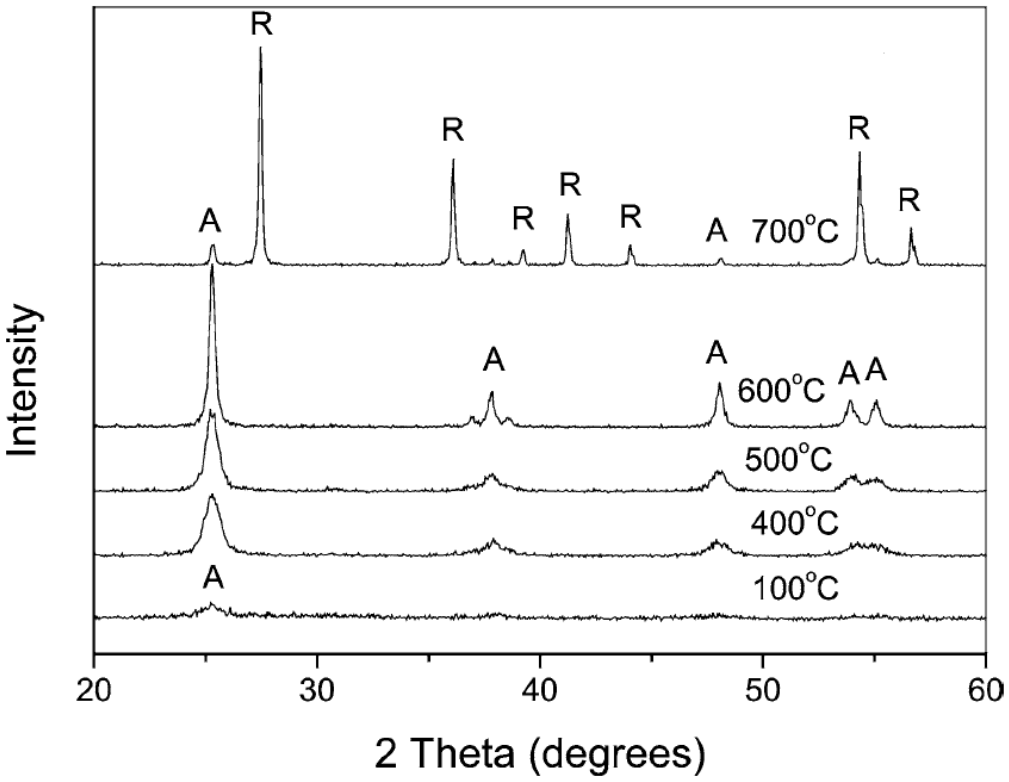

Figure 9. Evolution of the XRD pattern of a TiO_2 sample peptized with NH_4OH and calcined at different temperatures, from [91]. The A and R labels stand for anatase and rutile phases, respectively (reproduced with permission from J. Yu et al., Journal of Catalysis; published by Elsevier, 2003).

In [50,54,59,90,103,116,140,151], the hydrothermal treatment allows the increase of the crystallite size of the crystalline phase present in the as-synthesized sample. An increase of the duration, or temperature, of the hydrothermal treatment leads to larger crystallite size [50,55]. An as-synthesized anatase phase can also be converted into the rutile phase if the temperature or duration is sufficient, as illustrated in Figure 10, while an as-synthesized anatase/brookite mixture is converted to rutile phase after hydrothermal treatment at 200 °C or 240 °C for 2 h.

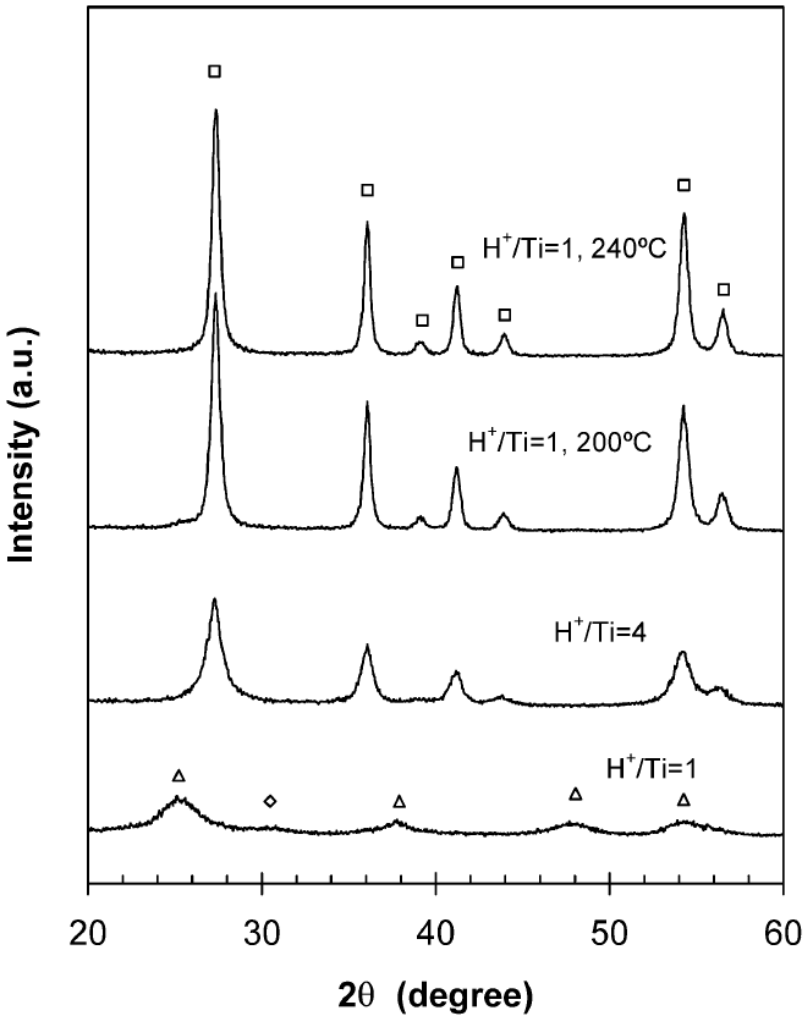

Figure 10. Evolution of the XRD pattern of a TiO_2 sample peptized with HNO_3 and hydrothermally treated at different temperatures, from [90]. (Δ) anatase, (◊), brookite, and (□) rutile phases (reproduced with permission from J. Yang et al., Journal of Colloid and Interface Science; published by Elsevier, 2005).

4. Morphology

Besides the crystallite formation at low temperature, colloidal aqueous TiO_2 synthesis allows the production of specific morphologies, depending on the synthesis conditions and the post-treatments applied. The following sections detail the TiO_2 morphologies obtained, depending on the same three synthetic steps: as-synthesized, and after calcination or hydrothermal treatments. The morphology is linked to the crystalline phase produced. The morphology depends on the crystalline phases produced during the synthesis. Indeed, anatase and brookite phases mainly lead to spherical nanoparticles, while rutile gives rod-like nanoparticles [104].

A particularity of this synthesis method using peptization is that the crystallite size and the nanoparticle size are the same. Indeed, it was shown in many studies [8,38,41,60,61,63,66,80] that one particle is made of one crystallite, thanks to comparisons made between XRD (crystallite size estimated by Scherrer formula) and TEM imaging.

4.1. Morphology of As-Synthesized Aqueous TiO_2

As-synthesized TiO_2 materials are stable colloids that are composed of nanoparticles in the range of 3–10 nm [96,100]. For the materials composed of anatase or an anatase/brookite mixture, all studies report similar spherical nanoparticles below 10 nm, as

shown in Figure 11a as an illustrative example [61]. When rutile phase is present, the morphology of rutile crystallites corresponds to nanorods, as depicted in Figure 11b [104]. Therefore, two main morphologies are observed, depending on the crystalline phases.

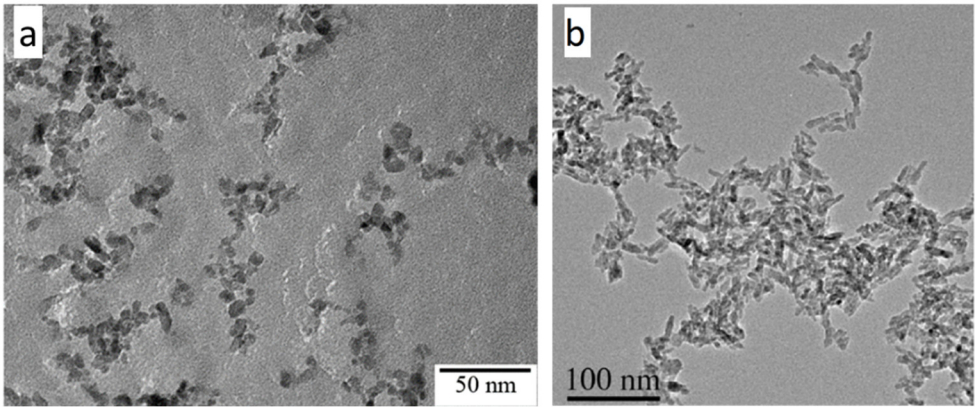

Figure 11. TEM micrographs of (**a**) TiO_2 anatase/brookite spherical nanoparticles, from [61] (reproduced with permission from J. G. Mahy et al., Journal of Photochemistry and Photobiology A: Chemistry; published by Elsevier, 2016) and (**b**) TiO_2 rutile nanorods, from [104] (reproduced with permission from S. Cassaignon et al., Journal of Physics and Chemistry of Solids; published by Elsevier, 2007).

The effect of PA on the final morphology of TiO_2 will depend on the crystalline phase that is formed during the synthesis. Indeed, when anatase and/or brookite phases are formed, spherical nanoparticles are produced. Basic or acidic PA can lead to anatase/brookite phases, and thus basic or acidic PA can lead to spherical nanoparticles. When organic acid PA is used, spherical nanoparticles are produced because only anatase phase is formed. When rutile is produced, a nanorod morphology is obtained and, globally, it is when a large amount of acidic PA is used that this is the case. Therefore, in conclusion, it is difficult to state that one type of PA (acidic or basic) will produce a specific type of morphology, but it is rather linked to the resulting crystalline phase.

4.2. Morphology of Aqueous TiO_2 after Calcination Treatment

As explained above, calcination permits further crystallizing the as-synthesized TiO_2 materials, yielding an increase in the crystallite size. Therefore, as for the as-synthesized materials, two morphologies (sphere [88] and nanorod [73]) are observed depending on the crystalline phases, but the size range of the nanoparticles is larger than the as-synthesized (10–70 nm vs. 2–10 nm). Figure 12 presents the spherical [43] and nanorod [73] morphologies obtained after calcination at 500 °C.

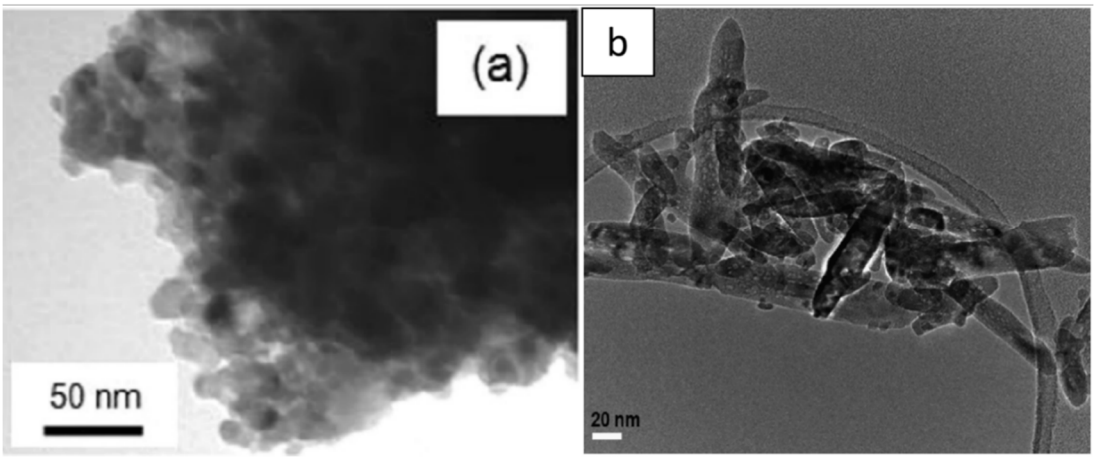

Figure 12. TEM micrographs of (**a**) TiO_2 anatase spherical sample calcined at 500 °C from [43] (reproduced with permission from F;.R. Cesconeto et al., Ceramics International; published by Elsevier, 2018) and (**b**) TiO_2 rutile nanorod sample calcined at 500 °C from [73] (reproduced with permission from P. Periyat et al., Materials Science in Semiconductor Processing; published by Elsevier, 2015).

4.3. Morphology of Aqueous TiO_2 after Hydrothermal Treatment

As for the calcination, the hydrothermal treatment allows the increase of the crystallite size (comprised between 10 and 80 nm), while keeping the morphology of the as-synthesized materials (sphere or nanorod) [83,152]. Figure 13 gives an example of spheres [50] and nanorods [141] obtained by hydrothermal treatment.

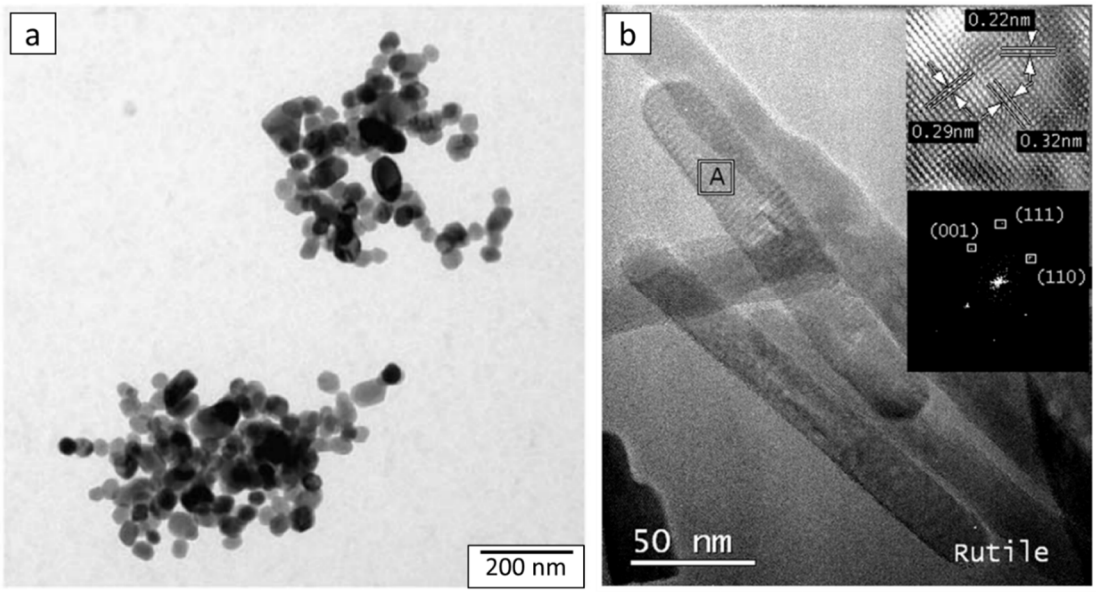

Figure 13. TEM micrographs of (**a**) TiO_2 anatase spherical sample hydrothermally treated at 230 °C from [50] (reproduced with permission from S. Hore et al., Journal of Materials Chemistry; published by RSC, 2005) and (**b**) TiO_2 rutile nanorod sample hydrothermally treated at 200 °C from [141] (reproduced with permission from H. Li et al., Materials Research Bulletin; published by Elsevier, 2011).

5. Doping and Additives

As mentioned in the introduction, the two intrinsic limitations of TiO_2 as a photocatalyst are (i) the fast charge recombination, and (ii) the high band gap value, which calls for UV light for activation [7]. Therefore, the doping and/or modification of colloidal aqueous TiO_2 are also described in the literature to prevent these limitations. Throughout the liter-

ature, four main modification strategies of aqueous TiO_2 were found: doping with (i) metallic or (ii) non-metallic species, (iii) a combination with other semiconductors, and (iv) sensitization with dye molecules.

The modification of TiO_2 with metallic species introduces metallic ions or metallic nanoparticles into the material. Metallic ions can produce intermediate levels of energy between the valence and conduction bands of TiO_2, leading to a reduction of the energy necessary for electron photoexcitation. As a consequence, near-visible light can activate the photocatalytic process. These metallic ions can also act as photoelectron-hole traps, increasing the recombination time and enhancing the electron–hole separation. Metallic nanoparticles dispersed in the TiO_2 matrix also act as electron traps due to their conductive nature. The metallic species listed are Ag [84,99,149], Fe [42,61,73], Cu [8,61], Rh [93], Pd, Ca [43], Cr [61,66], Pt [51], Zn [8,61,124], Nd [110,111], Tb [132], Ce [44,109,120], Eu [117,126], and W [123].

The doping with non-metallic elements is usually conducted with N, P, or S, and can reduce the band gap by creating an intermediate band for the electrons between the conduction band and the valence band. This doping allows the use of less energetic light to activate TiO_2. Here, we mainly found N-doping (around 5 mol%), due to the frequent use of HNO_3 as a peptizing agent, even in the materials referenced as pure TiO_2. Supplementary sources of N were also used: mainly amine as trimethylamine [63,95,127,133], urea [54,63], melamine [116], hydrazine [133], ethylene diamine [63,75], etc. Many studies reported photoactivity under near-visible range illumination (see Section 6). The combination with other semiconductors in heterojunction is also reported: with ZrO_2 [65,67], g-C_3N_4 [135], SnO [131], and Bi_2O_3 [77]. This modification produces a heterojunction at the interface of the two materials, which enhances the electron–hole separation due to the difference in energy levels of the conduction and valence bands of the two photocatalysts.

The introduction of dyes is reported in Mahy et al. [16]. In this case, the grafting of the porphyrin molecule at the surface allows the TiO_2 activation in the visible range, due to the transfer of electrons from the dye by its excitation under visible illumination [16]. One study reports the production of composites made of aqueous TiO_2 with carbon nanotubes [56]. In this case, the role of the carbon materials is similar to the introduction of metallic nanoparticles. As a carbon nanotube is a conductive material, it can trap the photo-generated electrons and decrease the recombination process.

6. Photocatalytic Properties

It is shown in the above paragraphs that colloidal aqueous TiO_2 synthesis can produce crystalline TiO_2 materials with specific morphologies, even without any thermal treatment. These crystalline materials are mainly being used for pollutant degradation. This section will summarize the photocatalytic activity of these aqueous TiO_2 materials identified in the literature. A fraction of the articles dealing with aqueous TiO_2 do not explore its photocatalytic properties and are limited to the description of the physicochemical properties. This represents 47 out of 115 articles, but in 10 cases, another application is also explored (see Section 7).

6.1. Photoactivity of As-Synthesized Aqueous TiO_2

Table 2 lists the parameters of the photocatalytic experiments in the studies using as-synthesized TiO_2 materials. The most tested molecule as a model "pollutant" is methylene blue (MB) [95,126,127,133,143], but 16 other molecules, such as methyl orange [125], p-nitrophenol [42], and rhodamine B [42,84,87], have also been tested, showing the versatility of this material. The majority of these "pollutants" are model molecules (dyes); photocatalytic degradations of real wastewater or mixed pollutant solutions are very rare. The pollutant concentration is kept low as the photocatalysis process is a finishing water treatment step to remove residual pollution if still present, for example, after a classical wastewater treatment plant. Concerning the illumination, the information is often not very complete. Indeed, sometimes the wavelength and/or the intensity are not given.

Globally, UV-A light or visible light (~350–500 nm range) is used in most of the cases, as it corresponds to the band gap of TiO_2. The time of irradiation can vary from minutes [106,126] to hours [42,120], up to 24 h [42], and depends on the power of the lamp.

Various dopants or additives are added at the beginning of the reaction to increase the photodegradation and/or the adsorption spectrum. Classically, metallic dopants such as Ag [84,99] or Fe [42] are added to enhance the electron–hole separation. As explained above, N-doping allows the increase of the light absorption in the visible range, and thus increases the photoactivity in the visible range [63,127].

Different shapes of photocatalysts can be used: powder [106,126,138], film deposited on various substrates [97,119,135], or even fabric [74]. Numerous studies [42,65,95,133,138] compare their photocatalysts to the most famous commercial TiO_2, Evonik Aeroxide P25, which is produced by high-temperature process. Usually, similar or better activities are obtained with the aqueous TiO_2. A direct comparison between all studies is very complicated, as the experimental conditions are different from one paper to another. Indeed, the lamp, illumination duration, concentration of photocatalyst or pollutant, and type of pollutant are the major parameters which differ from study to study (Table 2). Nevertheless, the high specific surface area obtained with the aqueous sol–gel process is referred to in most studies as the main reason for the increased photocatalytic activity compared to Evonik P25 (250 $m^2 g^{-1}$ for aqueous sol–gel samples vs. 50 $m^2 g^{-1}$ for P25). Therefore, the specific structure made of small nanoparticles (<10 nm, see Figure 10 from [8]) highly dispersed in water medium seems to play the most important role in its photocatalytic properties for pollutant removal in water.

Table 2 demonstrates that it is possible to obtain a very efficient TiO_2 material with an eco-friendly and easy synthesis without any additional high-temperature treatment. Indeed, the anatase phase, which is known to be the most efficient photocatalytic phase of TiO_2, due to its better charge separation efficiency, is easily produced.

Table 2. Parameters of photocatalytic experiments in studies using as-synthesized TiO_2 materials.

Paper	Photocatalyst and Shape (Concentration)	Pollutant (Concentration)	Illumination and Time	Best Degradation Results
Bazrafshan et al., 2015 [106]	• Pure TiO_2 • Powder (0.5 g/L)	Reactive orange dye (200 ppm)	Xenon lamp—40 min	100%
Belet et al., 2019 [124]	• Pure TiO_2, TiO_2/Zn • Film on glass	• Methylene blue (MB) (5×10^{-5} M) • pharma products (lorazepam, tramadol, alprazolam, ibuprofen, and metformin. 10 μg/L each)	254 nm—4 h	• 60% on MB • 10–50% on different pharma products
Bergamonti et al., 2014 [125]	• Pure TiO_2 • Powder (9.22 mM)	• Methyl orange (MO) (0.03 mM) • MB (0.03 mM)	365 nm—160 min	100% on both
Borlaf et al., 2014 [126]	• Pure TiO_2, TiO_2/Eu • Powder (0.33×10^{-2} M)	MB (0.33×10^{-2} M)	254 or 312 or 365 nm—40 min	Only kinetic constants given
Gole et al., 2004 [133]	• N/TiO_2 • Powder (5 g/L)	MB (--)	• 390 nm—600 min • 540 nm—600 min	• 80% at 390 nm • 23% at 540 nm
Chen et al., 2005 [95]	• N/TiO_2	MB (--)	• 390 nm—600 min	• 80%

	• Powder (5 g/L)		• 540 nm—600 min • 780 nm—600 min	• 25% • 5%
Douven et al., 2020 [42]	• Pure TiO_2, N, Fe doping • Powder (1 g/L) • Film on steel	• p-nitrophenol (PNP) (10^{-4} M) • Rhodamine B (RB) (2.5×10^{-6} M)	• Visible (400–800)—24 h • 395 nm (LED)—120 min	• 65% • 95%
Hu et al., 2005 [97]	• Pure TiO_2 • Film on quartz	Reactive brilliant red dye XB3 (50 mg/L)	365 nm—120 min	100%
Hu et al., 2014 [127]	• Pure TiO_2, N/TiO_2 • Powder (0.5 g/L)	MB (20 μM)	• UV—90 min • Visible (>420 nm)—300 min	• 75% (UV) • 65% (visible)
Huang et al., 2019 [135]	• gC_3N_4/TiO_2 • Composite film	NO_x (gas phase- 400 ppb)	Visible—cycle of 30 min	25% for one cycle
Kanna et al., 2008 [107]	• Pure TiO_2 • Powder (0.5 g/L)	• MB (2.5×10^{-5} M) • Cristal violet (CV) (2.5×10^{-5} M) • Congo red (CR) (2.5×10^{-5} M)	366 nm—3 h	• 90% • 95% • 100%
Léonard et al., 2016 [56]	• TiO_2/Nanotube • Film on glass	PNP (10^{-4} M)	• 365 nm—24 h • Visible (400–800 nm)—24 h	• 55% • 0%
Li et al., 2014 [115]	• Composite TiO_2/PSS or PEI • Powder (1 g/L)	• MB (10 mg/L) • RB (10 mg/L)	365 nm—280 or 400 min	• 95% • 97%
Liu et al., 2008 [119]	• Pure TiO_2 • Powder (0.5 g/L) • Film on aluminum and film on glass	• RB (liquid phase- 10 mg/L) • CH_3SH (gas phase—100 ppmv) • HCHO (gas phase—5.5 ppmv)	• 50 min—365 nm • 25 min—365 nm • 3 h—365 nm	• 95% • 97% • 85%
Liu et al., 2010 [120]	• Pure TiO_2, TiO_2/Ce^{3+} • Powder (1 g/L) • Film on filter paper	• MB (10 mg/L) • 2,3-dichlorophenol (10 mg/L) • Benzene (gas phase 5.5 ppmv)	• UV-A (365 nm) and visible (>420 nm) for liquid—50–180 min • 365,405,430,540,580 nm for gas—7–10 h	• 95–70% • 100–70% • 70–15%
Mahy et al. [16,41,61,62,64,65]	• Pure TiO_2, various doping (N, metallic ions, Zr, Pt, porphyrin) • Powder (1 g/L) • Film on prepainted steel	• PNP (10^{-4} M) • MB (2×10^{-5} M)	• UV-visible (300–800 nm)—8 h • Visible (400–800)—24 h • 365 nm—17 h	• 95% • 70% • 80%
Malengreaux et al. [8,66]	• Pure TiO_2, various doping (metallic ions) • Powder (1 g/L)	PNP (10^{-4} M)	UV-visible (300–800 nm)—7 h	75%
Qi et al., 2010 [74]	• Pure TiO_2 • Film on cotton fabric	Neolan Blue 2G (0.2 g/L)	365 nm—2 h	70%

Sharma et al., 2020 [138]	• Pure TiO_2 • Powder (0.01—0.35 M)	Solophenyl green (3.15 g/L)	365 nm—350 min	70%
Suligoj et al., 2016 [121]	• Pure TiO_2 • Composite film with SiO_2 on glass	Toluene (gas phase 49 ppmv)	365 nm—100 min	100%
Sung-Suh et al., 2004 [84]	• Pure TiO_2, TiO_2/Ag • Powder (0.4—4 g/L)	RB (10^{-5} M)	• UV—1 h • Visible—4 h	• 95% • 90%
Vinogradov et al., 2014 [87]	• Pure TiO_2 • Film on glass	RB (40 mg/L)	UV—120 min	95%
Wang et al., 2009 [99]	• Pure TiO_2, TiO_2/Ag • Powder (1 g/L)	MB (30 μM)	UV—90 min	55%
Wang et al., 2005 [143]	• Pure TiO_2 • Powder (0.09 M)	MB (0.016 g/L)	UV—25 min	45%
Xie et al., 2005 [110]	• Pure TiO_2, TiO_2/Nd^{3+} • Powder (1 g/L)	X3B (100 mg/L)	400–800 nm—120 min	90%
Yan et al., 2013 [131]	• Pure TiO_2, TiO_2/Sn • Powder (0.28 g/L)	MB (16 mg/L)	Visible (>420 nm)—100 min	45%
Yun et al., 2004 [92]	• Pure TiO_2 • Film on glass	Ethanol (gas phase 450 ppmv)	UV—50 min	100%
Zhang et al., 2001 [122]	• Pure TiO_2 • Powder (0.8 g/L)	sodium benzenesulfate (12 mM)	UV—4 h	100%

6.2. Photoactivity of Aqueous TiO_2 after a Calcination Treatment

Table 3 summarizes the parameters of the photocatalytic experiments for the studies using calcined aqueous TiO_2 materials. The observations are similar to Section 6.1 above: numerous pollutants can be degraded (but mainly model pollutants are studied, such as methylene blue), several efficient dopants are used to increase photo-degradation, and the various experimental conditions do not allow a direct comparison of the results. Nevertheless, the photoactivity of the calcined materials does not seem to be better than the as-synthesized materials. Indeed, similar degradation rates are obtained with similar illumination times (compare Table 3 vs. Table 2).

Table 3. Parameters of photocatalytic experiments for studies using calcined aqueous TiO_2 materials.

Paper	Photocatalyst and Shape (Concentration)	Pollutant (Concentration)	Illumination and Time	Best Degradation Results
Al-Maliki et al., 2017 [132]	• Pure TiO_2, TiO_2/Tb • Film	$KMnO_4$ (2×10^{-5} M)	• UV (200–400 nm)—75 min • 400–600 nm—75 min	• 65% • 50%
Borlaf et al., 2012 [93]	• Pure TiO_2, TiO_2/Rh^{3+} • Powder (0.33×10^{-2} M)	MB (0.33×10^{-2} M)	254 or 312 or 365 nm—40 min	Only kinetic constants given
Cano-Franco et al., 2019 [44]	• Pure TiO_2, TiO_2/Ce • Powder (1 g/L)	MB (400 ppm)	Solar lamp (Xe lamp)—150 min	98%
Cesconeto et al., 2018 [43]	• Pure TiO_2, TiO_2/Ca • Powder (0.1 g/L)	MB (1.25×10^{-3} M)	254 or 312 or 365 nm—40 min	Only kinetic constants given
Chung et al., 2016 [134]	• Pure TiO_2 • Powder (0.1 g/L)	Dye reactive orange 16 (RO16) (25 ppm)	UV—120 min	100%
Haque et al., 2017 [49]	• Pure TiO_2 • Powder (0.5 g/L)	MB and MO (--)	Visible—120 min	70%
Ibrahim et al., 2010 [52]	• Pure TiO_2 • Powder (0.1 g)	MO (30 ppm)	UV—5 h	100%
Kattoor et al., 2014 [114]	• Pure TiO_2 • Powder (0.03 g)	MB (10^{-5} M)	UV-A—100 min	85%
Khan et al., 2017 [129]	• Pure TiO_2 • Powder (0.063 g/L)	PNP (0.02 g/L)	254 nm—30 min	65%
Ma et al., 2012 [117]	• Pure TiO_2, TiO_2/Eu • Powder (1 g/L)	Salicylic acid (50 mg/L)	Visible (>420 nm)—300 min	88%
Mahmoud et al., 2018 [34]	• Pure TiO_2 • Powder (1 g/L)	• MB (10 ppm) • PNP • CV	UV—120 min	100%
Mao et al., 2005 [130]	• Pure TiO_2 • Powder (0.3 g/L)	X3B (30 mg/L)	UV—40 min	100%
Maver et al., 2009 [67]	• Pure TiO_2, TiO_2/Zr • Film on glass and silicon	Plasmocorinth B (40 mg/L)	UV-A—3000 s	70%
Molea et al., 2014 [105]	• Pure TiO_2 • Powder (0.1 g/L)	MB (2.75×10^{-3} g/L)	300–400 nm + 400–700 nm—300 min	47%
Mutuma et al., 2015 [70]	• Pure TiO_2 • Powder (0.6 g/L)	MB (32 mg/L)	UV—70 min	95%
Periyat et al., 2015 [73]	• Pure TiO_2, TiO_2/Fe • Powder (1.2 g/L)	R6G (5×10^{-6} M)	420–800 nm—20 min	100%
Qiu et al., 2007 [75]	• Pure TiO_2, TiO_2/N	MB (--)	Visible (>400 nm)—350 min	85%

	• Powder (11 mg/L)			
Quintero et al., 2020 [76]	• Pure TiO_2 • Powder (1 g/L)	MB (5 ppm)	365 nm—250 min	90%
Ropero-Vega et al., 2019 [77]	• Pure TiO_2, TiO_2/Bi_2O_3 • Film on glass	Salicylic acid (0.1 mM)	UV-Visible (325–650 nm) —1 h	10%
Su et al., 2004 [98]	• Pure TiO_2 • Powder (--)	Salicylic acid (4×10^{-4} M)	254 nm—250 min	65%
Tobaldi et al., 2014 [85]	• Pure TiO_2 • Powder (0.25 g/L) • Film on petri dishes	MB (liquid phase—5 mg/L) NO_x (gas phases—0.5 ppmv)	Solar light—7 h Solar light—40 min	100% 60%
Xie et al., 2005 [111]	• Pure TiO_2, TiO_2/Nd • Powder (1 g/L)	X3B (100 mg/L)	365 nm + 400–800 nm—120 min 400–800 nm—120 min	95% 35%
Yamazaki et al., 2001 [89]	• Pure TiO_2 • Powder (0.2 g)	Ethylene (gas phase 160 ppmv)	4W fluorescence black light bulbs—2 h	100%
Yu et al., 2003 [91]	• Pure TiO_2 • Film on petri dishes (0.3 g)	Acetone (gas phase—400 ppm)	365 nm—60 min	Only kinetic constants given

6.3. Photoactivity of Aqueous TiO_2 after Hydrothermal Treatment

Table 4 summarizes the parameters of the photocatalytic experiments for the studies using aqueous TiO_2 materials after a hydrothermal treatment. As for the calcined TiO_2 materials, the photoactivity does not seem to be improved compared to the as-synthesized materials (compare Table 4 vs. Table 2). In terms of photoactivity, it can be deduced that a thermal treatment (calcination or hydrothermal) is not necessary to obtain an efficient photocatalyst with this type of synthesis method. Indeed, before thermal treatment, crystalline materials are already present with a high specific surface area. The thermal treatment increases the crystallite size and allows a 100% crystalline material to be obtained, but reduces the specific surface area, hence it is not advantageous because photocatalysis occurs at the surface.

One study [151] tested the photo efficiency of their catalysts on real wastewater, where multiple pollutants were present as pharmaceutical products, pesticides, and various organic chemicals. This study showed the effectiveness of the TiO_2 photocatalysts for the degradation of these molecules.

Table 4. Parameters of photocatalytic experiments for studies using aqueous TiO_2 materials after hydrothermal treatment.

Paper	Photocatalyst and Shape (Concentration)	Pollutant (Concentration)	Illumination and Time	Best Degradation Results
Fallet et al., 2006 [150]	• Pure TiO_2 • Film on Si wafer	Malic acid (3.7×10^{-4} M)	UV (>340 nm)—3 h	90%
Jiang et al., 2011 [128]	• Pure TiO_2 • Powder (1 g/L)	MO (10 mg/L)	Visible (>400 nm)—100 min	35%
Kaplan et al., 2016 [54]	• Pure TiO_2 • Powder (0–125 mg/L)	Bisphenol A (BPA) (10 mg/L)	365 nm—60 min	100%
Liu et al., 2014 [116]	• Pure TiO_2, TiO_2/N • Film on glass	HCHO (gas phase—0.32 mg/m^3)	Visible ()—24 h	95%
Mahata et al., 2012 [59]	• Pure TiO_2 • Powder (--)	MO (--)	UV Visible—120 min	85%
Saif et al., 2012 [151]	• Pure TiO_2 • Powder (--)	Real wastewater	Solar light—3 h	57% mineralization
Xie et al., 2003 [109]	• Pure TiO_2, TiO_2/Ce • Powder (1 g/L)	X3B (100 mg/L)	400–800 nm—120 min	95%

7. Addition Features for Aqueous Sol–Gel TiO_2

Some other studies used colloidal aqueous TiO_2 materials in applications other than photocatalytic pollutant degradation. All these applications used the other properties of titania, such as its hydrophilicity, its high refractive index, or its semi-conducting property. In Alcober et al. [123], aqueous TiO_2 material is utilized to produce photochromic coatings with tungsten doping. In Antonello et al. [139], high refractive index coatings are produced from aqueous TiO_2 suspensions. In Bugakova et al. [94], TiO_2 inks, based on aqueous TiO_2 colloids, are used for applications derived from the inkjet printing of microstructures for electronic devices. In Haq et al. [48] and Lin et al. [153], aqueous TiO_2 suspensions give adsorbent materials for heavy metals and dye adsorption. Indeed, as aqueous synthesis of TiO_2 suspensions produces TiO_2 nanoparticles, the specific surface area of these materials is high compared to titania obtained by high-temperature synthesis. In Hore et al. [50] and Kashyout et al. [55], aqueous TiO_2 materials are used in solar cell fabrication. In Papiya et al. [72], a cathode catalyst for microbial fuel cells is produced with aqueous TiO_2 materials. In Salahuddin et al. [79], aqueous TiO_2 is mixed with PLA to design a nanocomposite system for Norfloxacin drug delivery. Hydrophilic surfaces are also produced with aqueous TiO_2 [62,138]. The use of photocatalyst materials such as aqueous TiO_2 can be also implemented in energy related fields, such as the production of H_2 by photocatalyzed decomposition of water [154]. The possibility of integrating heterogeneous photocatalysis with electrochemical processes to exploit their synergistic actions can be also envisaged [155]. Numerous further studies can be imagined to explore fully the properties of this green TiO_2 synthesis pathway.

8. Conclusions and Outlook

The aim of this review was to establish the state of the art of the research in the area of the little known eco-friendly process of producing TiO_2 via colloidal aqueous sol–gel synthesis, resulting in a crystalline material without a calcination step. From 1987 to 2020, about 115 articles were found dealing with colloidal aqueous sol–gel TiO_2 preparation, taking into account three types of aqueous TiO_2: the as-synthesized type obtained directly

after synthesis, without any specific treatment; the calcined, obtained after a subsequent calcination step; and the hydrothermal, obtained after this specific autoclave treatment.

This eco-friendly process is based on the hydrolysis of a Ti precursor in excess of water, followed by the peptization of the precipitated TiO_2. Compared to classical TiO_2 synthesis, this colloidal aqueous sol–gel method results in crystalline TiO_2 nanoparticles without a thermal treatment, and it is a green synthesis method because it uses small amounts of chemicals, water as a solvent, and a low temperature for crystallization. Moreover, some works have shown that this synthesis method can be easily upscaled to 20 L.

Depending on the synthesis parameters, the three crystalline phases of TiO_2 (anatase, brookite, rutile) can be obtained. The morphology of the nanoparticles can also be tailored by the synthesis parameters. The most important parameter is the peptizing agent. Indeed, depending on its acidic or basic character and also on its amount, it can modulate the crystallinity, and so, the morphology of the material. HNO_3 seems to be the most versatile PA. Indeed, it allows obtaining the three different phases of TiO_2 and the corresponding morphologies (nanosphere or nanorod) just by changing its quantity during the synthesis.

The exact mechanism of the TiO_2 material formation and the exact influence of the PA on the resulting TiO_2 materials needs deeper studies, to understand clearly the formation of the different crystalline phases and morphologies. For example, the use of in-situ XRD or FTIR to probe the exact formation mechanism of PA-assisted sol–gel synthesis of TiO_2 could be a path to explore. Moreover, machine learning and big data analysis will open a new avenue in this TiO_2 material research. Indeed, they could help to find a correlation between the many different experimental parameters and their ability to produce highly crystalline TiO_2.

Even if crystalline TiO_2 materials are obtained after aqueous sol–gel synthesis, some studies apply a thermal post-treatment, calcination, or hydrothermal to further crystallize the materials. These treatments can also increase the crystallite size of the as-synthesized material and modify its morphology. Moreover, the surface area will decrease during the calcination due to particle growth with the phase change. Furthermore, the increase in the calcination temperature causes the particles to coalesce, creating tightly connected agglomerates, blocking the entry of N_2 gas during the BET analysis.

The aqueous TiO_2 photocatalysts are mainly used in various photocatalytic reactions for organic pollutant degradation. More than 20 different molecules have been reported to be degraded with these materials, but mainly model pollutants. Experiments on real wastewater are lacking in the literature for this type of material. The numerous experimental conditions make it difficult to compare the performance of catalysts. Nevertheless, the as-synthesized materials seem to have an equivalent photocatalytic efficiency to the photocatalysts post-treated with thermal treatments. Indeed, as-prepared, the TiO_2 photocatalysts are crystalline and present a high specific surface area. Thermal treatments do not seem to be necessary from a photocatalytic point of view. Moreover, studies showed that aqueous TiO_2 presents better photoactivity than commercial Evonik Aeroxide P25, which is produced by high-temperature process.

Emerging applications are also referenced, such as elaborating catalysts for fuel cells, nanocomposite drug delivery systems, or the inkjet printing of microstructures. As the development of alternative energy sources is very prominent in current research activities, the use of this kind of photocatalyst to produce H_2 from the photocatalyzed decomposition of water also seems a promising path to explore. Moreover, the development of electrophotocatalytic devices for various applications, in water pollution treatment for example, will be realized in the next few years. However, only a few works have explored these other properties, giving a lot of potential avenues for studying this eco-friendly TiO_2 synthesis method for innovative implementations.

Author Contributions: Writing—original draft preparation, J.G.M., L.L., T.H., S.D.L., R.H.M.M., C.-A.F., S.H.; writing—review and editing, J.G.M., L.L., T.H., S.D.L., R.H.M.M., C.-A.F., S.H. All authors have read and agreed to the published version of the manuscript.

Funding: This research was funded by INNOVIRIS Brussels (Institute for Research and Innovation) through the Bridge project platform —as part of COLORES project.

Data Availability Statement: All data were taken from the articles of the bibliography section.

Acknowledgments: S.D.L. and S.H. are grateful to F.R.S.-F.N.R.S. for their Senior Research Associate position. J.G.M., R.H.M.M., C.A.F. and S.H. also thank INNOVIRIS Brussels for financial support through the Bridge project—COLORES.

Conflicts of Interest: The authors declare no conflict of interest.

References

1. Oturan, M.A.; Aaron, J.-J. Advanced Oxidation Processes in Water/Wastewater Treatment: Principles and Applications. A Review. *Crit. Rev. Environ. Sci. Technol.* **2014**, *44*, 2577–2641, doi:10.1080/10643389.2013.829765.
2. Nakata, K.; Fujishima, A. TiO2 photocatalysis: Design and applications. *J. Photochem. Photobiol. C Photochem. Rev.* **2012**, *13*, 169–189, doi:10.1016/j.jphotochemrev.2012.06.001.
3. Hermawan, A.; Hanindriyo, A.T.; Ramadhan, E.R.; Asakura, Y.; Hasegawa, T.; Hongo, K.; Inada, M.; Maezono, R.; Yin, S. Octahedral morphology of NiO with (111) facet synthesized from the transformation of NiOHCl for the NOx detection and degradation: Experiment and DFT calculation. *Inorg. Chem. Front.* **2020**, *7*, 3431–3442, doi:10.1039/d0qi00682c.
4. Ong, C.B.; Ng, L.Y.; Mohammad, A.W. A review of ZnO nanoparticles as solar photocatalysts: Synthesis, mechanisms and applications. *Renew. Sustain. Energy Rev.* **2018**, *81*, 536–551.
5. Ma, R.; Zhang, S.; Wen, T.; Gu, P.; Li, L.; Zhao, G.; Niu, F.; Huang, Q.; Tang, Z.; Wang, X. A critical review on visible-light-response CeO2-based photocatalysts with enhanced photooxidation of organic pollutants. *Catal. Today* **2019**, *335*, 20–30, doi:10.1016/j.cattod.2018.11.016.
6. Chiam, S.-L.; Pung, S.-Y.; Yeoh, F.-Y. Recent developments in MnO2-based photocatalysts for organic dye removal: A review. *Environ. Sci. Pollut. Res.* **2020**, *27*, 5759–5778, doi:10.1007/s11356-019-07568-8.
7. Pelaez, M.; Nolan, N.T.; Pillai, S.C.; Seery, M.; Falaras, P.; Kontos, A.G.; Dunlop, P.S.; Hamilton, J.W.; Byrne, J.; O'Shea, K.; et al. A review on the visible light active titanium dioxide photocatalysts for environmental applications. *Appl. Catal. B Environ.* **2012**, *125*, 331–349, doi:10.1016/j.apcatb.2012.05.036.
8. Malengreaux, C.M.; Douven, S.; Poelman, D.; Heinrichs, B.; Bartlett, J.R. An ambient temperature aqueous sol–gel processing of efficient nanocrystalline doped TiO2-based photocatalysts for the degradation of organic pollutants. *J. Sol Gel Sci. Technol.* **2014**, *71*, 557–570, doi:10.1007/s10971-014-3405-6.
9. Espino-Estévez, M.; Fernández-Rodríguez, C.; González-Díaz, O.M.; Araña, J.; Espinós, J.; Ortega-Méndez, J.; Doña-Rodríguez, J.M. Effect of TiO2–Pd and TiO2–Ag on the photocatalytic oxidation of diclofenac, isoproturon and phenol. *Chem. Eng. J.* **2016**, *298*, 82–95, doi:10.1016/j.cej.2016.04.016.
10. Vaiano, V.; Iervolino, G.; Sannino, D.; Murcia, J.J.; Hidalgo, M.C.; Ciambelli, P.; Navío, J.A. Photocatalytic removal of patent blue V dye on Au-TiO2 and Pt-TiO2 catalysts. *Appl. Catal. B Environ.* **2016**, *188*, 134–146, doi:10.1016/j.apcatb.2016.02.001.
11. Di Paola, A.; Marci, G.; Palmisano, L.; Schiavello, M.; Uosaki, K.; Ikeda, A.S.; Ohtani, B. Preparation of Polycrystalline TiO2Photocatalysts Impregnated with Various Transition Metal Ions: Characterization and Photocatalytic Activity for the Degradation of 4-Nitrophenol. *J. Phys. Chem. B* **2002**, *106*, 637–645, doi:10.1021/jp013074l.
12. Rauf, M.; Meetani, M.; Hisaindee, S. An overview on the photocatalytic degradation of azo dyes in the presence of TiO2 doped with selective transition metals. *Desalination* **2011**, *276*, 13–27, doi:10.1016/j.desal.2011.03.071.
13. Bodson, C.J.; Heinrichs, B.; Tasseroul, L.; Bied, C.; Mahy, J.G.; Man, M.W.C.; Lambert, S.D. Efficient P- and Ag-doped titania for the photocatalytic degradation of waste water organic pollutants. *J. Alloys Compd.* **2016**, *682*, 144–153, doi:10.1016/j.jallcom.2016.04.295.
14. Di Valentin, C.; Pacchioni, G.; Selloni, A.; Livraghi, S.; Giamello, E. Characterization of Paramagnetic Species in N-Doped TiO2 Powders by EPR Spectroscopy and DFT Calculations. *J. Phys. Chem. B* **2005**, *109*, 11414–11419, doi:10.1021/jp051756t.
15. Gilma, G.O.; Carlos, A.P.M.; Fernando, M.O.; Edgar, A.P.-M. Photocatalytic degradation of phenol on TiO2 and TiO2/Pt sensitized with metallophthalocyanines. *Catal. Today* **2005**, *107–108*, 589–594, doi:10.1016/j.cattod.2005.07.021.
16. Mahy, J.G.; Paez, C.A.; Carcel, C.; Bied, C.; Tatton, A.S.; Damblon, C.; Heinrichs, B.; Man, M.W.C.; Lambert, S.D. Porphyrin-based hybrid silica-titania as a visible-light photocatalyst. *J. Photochem. Photobiol. A Chem.* **2019**, *373*, 66–76, doi:10.1016/j.jphotochem.2019.01.001.
17. Xie, H.; Gao, G.; Tian, Z.; Bing, N.; Wang, L. Synthesis of TiO2 nanoparticles by propane/air turbulent flame CVD process. *Particuology* **2009**, *7*, 204–210, doi:10.1016/j.partic.2009.03.003.
18. Djenadic, R.; Winterer, M. Chemical Vapor Synthesis of Nanocrystalline Oxides. In *2D Nanoelectronics*; Springer Science and Business Media LLC: Berlin/Heidelberg, Germany, 2012; pp. 49–76.

19. Inturi, S.N.R.; Boningari, T.; Suidan, M.; Smirniotis, P.G. Flame Aerosol Synthesized Cr Incorporated TiO2for Visible Light Photodegradation of Gas Phase Acetonitrile. *J. Phys. Chem. C* **2013**, *118*, 231–242, doi:10.1021/jp404290g.
20. Dar, M.I.; Chandiran, A.K.; Graetzel, M.; Nazeeruddin, M.K.; Shivashankar, S.A. Controlled synthesis of TiO2 nanoparticles and nanospheres using a microwave assisted approach for their application in dye-sensitized solar cells. *J. Mater. Chem. A* **2013**, *2*, 1662–1667, doi:10.1039/c3ta14130f.
21. Zhang, D.; Qi, L.; Ma, J.; Cheng, H. Formation of crystalline nanosized titania in reverse micelles at room temperature. *J. Mater. Chem.* **2002**, *12*, 3677–3680, doi:10.1039/b206996b.
22. Nian, J.-N.; Teng, H. Hydrothermal Synthesis of Single-Crystalline Anatase TiO2Nanorods with Nanotubes as the Precursor. *J. Phys. Chem. B* **2006**, *110*, 4193–4198, doi:10.1021/jp0567321.
23. Simon, P.; Pignon, B.; Miao, B.; Coste-Leconte, S.; Leconte, Y.; Marguet, S.; Jegou, P.; Bouchet-Fabre, B.; Reynaud, C.; Herlin-Boime, N. N-Doped Titanium Monoxide Nanoparticles with TiO Rock-Salt Structure, Low Energy Band Gap, and Visible Light Activity. *Chem. Mater.* **2010**, *22*, 3704–3711, doi:10.1021/cm100653q.
24. Gratzel, M. Sol-Gel Processed TiO2 Films for Photovoltaic Applications. *J. Sol Gel Sci. Technol.* **2001**, *22*, 7–13, doi:10.1023/a:1011273700573.
25. Carp, O. Photoinduced reactivity of titanium dioxide. *Prog. Solid State Chem.* **2004**, *32*, 33–177, doi:10.1016/j.progsolidstchem.2004.08.001.
26. Huang, T.; Huang, W.; Zhou, C.; Situ, Y.; Huang, H. Superhydrophilicity of TiO2/SiO2 thin films: Synergistic effect of SiO2 and phase-separation-induced porous structure. *Surf. Coat. Technol.* **2012**, *213*, 126–132, doi:10.1016/j.surfcoat.2012.10.033.
27. Guan, K. Relationship between photocatalytic activity, hydrophilicity and self-cleaning effect of TiO2/SiO2 films. *Surf. Coat. Technol.* **2005**, *191*, 155–160, doi:10.1016/j.surfcoat.2004.02.022.
28. Antonelli, D.M.; Ying, J. Synthesis of Hexagonally Packed Mesoporous TiO2 by a Modified Sol–Gel Method. *Angew. Chem. Int. Ed.* **1995**, *34*, 2014–2017, doi:10.1002/anie.199520141.
29. Braconnier, B.; Páez, C.A.; Lambert, S.; Alié, C.; Henrist, C.; Poelman, D.; Pirard, J.-P.; Cloots, R.; Heinrichs, B. Ag- and SiO2-doped porous TiO2 with enhanced thermal stability. *Microporous Mesoporous Mater.* **2009**, *122*, 247–254, doi:10.1016/j.micromeso.2009.03.007.
30. Anderson, C.; Bard, A.J. An Improved Photocatalyst of TiO2/SiO2 Prepared by a Sol-Gel Synthesis. *J. Phys. Chem.* **1995**, *99*, 9882–9885, doi:10.1021/j100024a033.
31. Brinker, G.W.; Jeffrey, C.S. Sol-gel science. *The Physics and Chemistry of Sol-Gel Processing*; Academic Press: Cambridge, MA, USA, 2013.
32. Schubert, U. Chemical modification of titanium alkoxides for sol–gel processing. *J. Mater. Chem.* **2005**, *15*, 3701–3715, doi:10.1039/b504269k.
33. Jan, W.G. Encyclopedic Dictionary of Polymers. *Encycl. Dict. Polym.* **2011**, doi:10.1007/978-1-4419-6247-8.
34. Mahmoud, H.A.; Narasimharao, K.; Ali, T.T.; Khalil, K.M.S. Acidic Peptizing Agent Effect on Anatase-Rutile Ratio and Photocatalytic Performance of TiO2 Nanoparticles. *Nanoscale Res. Lett.* **2018**, *13*, 48, doi:10.1186/s11671-018-2465-x.
35. Yamanaka, S.; Nishihara, T.; Hattori, M.; Suzuki, Y. Preparation and properties of titania pillared clay. *Mater. Chem. Phys.* **1987**, *17*, 87–101, doi:10.1016/0254-0584(87)90050-2.
36. Anderson, M.A.; Gieselmann, M.J.; Xu, Q. Titania and alumina ceramic membranes. *J. Membr. Sci.* **1988**, *39*, 243–258, doi:10.1016/s0376-7388(00)80932-1.
37. Doeuff, S.; Henry, M.; Sanchez, C.; Livage, J. Hydrolysis of titanium alkoxides: Modification of the molecular precursor by acetic acid. *J. Non Cryst. Solids* **1987**, *89*, 206–216, doi:10.1016/s0022-3093(87)80333-2.
38. Mahshid, S.; Askari, M.; Ghamsari, M.S. Synthesis of TiO2 nanoparticles by hydrolysis and peptization of titanium isopropoxide solution. *J. Mater. Process. Technol.* **2007**, *189*, 296–300, doi:10.1016/j.jmatprotec.2007.01.040.
39. Bischoff, B.L.; Anderson, M.A. Peptization Process in the Sol-Gel Preparation of Porous Anatase (TiO2). *Chem. Mater.* **1995**, *7*, 1772–1778, doi:10.1021/cm00058a004.
40. Matijevic, E. Monodispersed metal (hydrous) oxides—A fascinating field of colloid science. *Acc. Chem. Res.* **1981**, *14*, 22–29, doi:10.1021/ar00061a004.
41. Mahy, J.G.; Deschamps, F.; Collard, V.; Jérôme, C.; Bartlett, J.; Lambert, S.D.; Heinrichs, B. Acid acting as redispersing agent to form stable colloids from photoactive crystalline aqueous sol–gel TiO2 powder. *J. Sol Gel Sci. Technol.* **2018**, *87*, 568–583, doi:10.1007/s10971-018-4751-6.
42. Douven, S.; Mahy, J.G.; Wolfs, C.; Reyserhove, C.; Poelman, D.; Devred, F.; Gaigneaux, E.M.; Lambert, S.D. Efficient N, Fe Co-Doped TiO2 Active under Cost-Effective Visible LED Light: From Powders to Films. *Catalysts* **2020**, *10*, 547, doi:10.3390/catal10050547.
43. Cesconeto, F.R.; Borlaf, M.; Nieto, M.I.; de Oliveira, A.P.N.; Moreno, R. Synthesis of CaTiO3 and CaTiO3/TiO2 nanoparticulate compounds through Ca^{2+}/TiO_2 colloidal sols: Structural and photocatalytic characterization. *Ceram. Int.* **2018**, *44*, 301–309, doi:10.1016/j.ceramint.2017.09.173.
44. Cano-Franco, J.C.; Álvarez-Láinez, M. Effect of CeO2 content in morphology and optoelectronic properties of TiO2-CeO2 nanoparticles in visible light organic degradation. *Mater. Sci. Semicond. Process.* **2019**, *90*, 190–197, doi:10.1016/j.mssp.2018.10.017.
45. Colomer, M.T.; Guzmán, J.; Moreno, R. Determination of Peptization Time of Particulate Sols Using Optical Techniques: Titania As a Case Study. *Chem. Mater.* **2008**, *20*, 4161–4165, doi:10.1021/cm703560x.

46. Colomer, M.T.; Guzmã¡n, J.; Moreno, R. Peptization of Nanoparticulate Titania Sols Prepared Under Different Waterâ€"Alkoxide Molar Ratios. *J. Am. Ceram. Soc.* **2009**, *93*, 59–64, doi:10.1111/j.1551-2916.2009.03294.x.
47. Ghamsari, M.S.; Gaeeni, M.R.; Han, W.; Park, H.-H. Highly stable colloidal TiO2 nanocrystals with strong violet-blue emission. *J. Lumin.* **2016**, *178*, 89–93, doi:10.1016/j.jlumin.2016.05.036.
48. Haq, S.; Rehman, W.; Waseem, M. Adsorption Efficiency of Anatase TiO2 Nanoparticles Against Cadmium Ions. *J. Inorg. Organomet. Polym. Mater.* **2018**, *29*, 651–658, doi:10.1007/s10904-018-1038-x.
49. Haque, F.Z.; Nandanwar, R.; Singh, P. Evaluating photodegradation properties of anatase and rutile TiO2 nanoparticles for organic compounds. *Optik* **2017**, *128*, 191–200, doi:10.1016/j.ijleo.2016.10.025.
50. Hore, S.; Palomares, E.; Smit, H.; Bakker, N.J.; Comte, P.; Liska, P.; Thampi, K.R.; Kroon, J.M.; Hinsch, A.; Durrant, J.R. Acid versus base peptization of mesoporous nanocrystalline TiO2 films: Functional studies in dye sensitized solar cells. *J. Mater. Chem.* **2004**, *15*, 412–418, doi:10.1039/b407963a.
51. Huang, B.-S.; Tseng, H.-H.; Su, E.-C.; Chiu, I.-C.; Wey, M.-Y. Characterization and photoactivity of Pt/N-doped TiO2 synthesized through a sol–gel process at room temperature. *J. Nanoparticle Res.* **2015**, *17*, 282, doi:10.1007/s11051-015-3091-5.
52. Ibrahim, S.A.; Sreekantan, S. Effect of pH on TiO2 Nanoparticles via Sol-Gel Method. *Adv. Mater. Res.* **2010**, *173*, 184–189, doi:10.4028/www.scientific.net/amr.173.184.
53. Khalil, K.M.; El-Khatib, R.M.; Ali, T.T.; Mahmoud, H.A.; Elsamahy, A.A. Titania nanoparticles by acidic peptization of xerogel formed by hydrolysis of titanium(IV) isopropoxide under atmospheric humidity conditions. *Powder Technol.* **2013**, *245*, 156–162, doi:10.1016/j.powtec.2013.04.023.
54. Kaplan, R.; Erjavec, B.; Dražić, G.; Grdadolnik, J.; Pintar, A. Simple synthesis of anatase/rutile/brookite TiO2 nanocomposite with superior mineralization potential for photocatalytic degradation of water pollutants. *Appl. Catal. B Environ.* **2016**, *181*, 465–474, doi:10.1016/j.apcatb.2015.08.027.
55. Kashyout, A.; Soliman, M.; Fathy, M. Effect of preparation parameters on the properties of TiO2 nanoparticles for dye sensitized solar cells. *Renew. Energy* **2010**, *35*, 2914–2920, doi:10.1016/j.renene.2010.04.035.
56. Léonard, G.L.-M.; Remy, S.; Heinrichs, B. Doping TiO2 films with carbon nanotubes to simultaneously optimise antistatic, photocatalytic and superhydrophilic properties. *J. Sol Gel Sci. Technol.* **2016**, *79*, 413–425, doi:10.1007/s10971-016-3975-6.
57. Leyva-Porras, C.; Toxqui-Teran, A.; Vega-Becerra, O.; Miki-Yoshida, M.; Rojas-Villalobos, M.; García-Guaderrama, M.; Aguilar-Martínez, J. Low-temperature synthesis and characterization of anatase TiO2 nanoparticles by an acid assisted sol–gel method. *J. Alloys Compd.* **2015**, *647*, 627–636, doi:10.1016/j.jallcom.2015.06.041.
58. Lim, C.S. Effect of pH on the Microstructural Morphology and Phase Transformation of TiO2 Nanopowders Prepared by Sol-Gel Method. *Asian J. Chem.* **2014**, *26*, 1843–1847, doi:10.14233/ajchem.2014.15831a.
59. Mahata, S.; Mahato, S.S.; Nandi, M.M.; Mondal, B. Synthesis of TiO[sub 2] nanoparticles by hydrolysis and peptization of titanium isopropoxide solution. *AIP Conf. Proc.* **2011**, *1461*, 225–228, doi:10.1063/1.4736892.
60. Mahshid, S.; Askari, M.; Ghamsari, M.S.; Afshar, N.; Lahuti, S. Mixed-phase TiO2 nanoparticles preparation using sol–gel method. *J. Alloys Compd.* **2009**, *478*, 586–589, doi:10.1016/j.jallcom.2008.11.094.
61. Mahy, J.G.; Lambert, S.D.; Léonard, G.L.-M.; Zubiaur, A.; Olu, P.-Y.; Mahmoud, A.; Boschini, F.; Heinrichs, B. Towards a large scale aqueous sol-gel synthesis of doped TiO2: Study of various metallic dopings for the photocatalytic degradation of p-nitrophenol. *J. Photochem. Photobiol. A Chem.* **2016**, *329*, 189–202, doi:10.1016/j.jphotochem.2016.06.029.
62. Mahy, J.G.; Léonard, G.L.-M.; Pirard, S.; Wicky, D.; Daniel, A.; Archambeau, C.; Liquet, D.; Heinrichs, B. Aqueous sol–gel synthesis and film deposition methods for the large-scale manufacture of coated steel with self-cleaning properties. *J. Sol Gel Sci. Technol.* **2017**, *81*, 27–35, doi:10.1007/s10971-016-4020-5.
63. Mahy, J.G.; Cerfontaine, V.; Poelman, D.; Devred, F.; Gaigneaux, E.M.; Heinrichs, B.; Lambert, S.D. Highly Efficient Low-Temperature N-Doped TiO2 Catalysts for Visible Light Photocatalytic Applications. *Materials* **2018**, *11*, 584, doi:10.3390/ma11040584.
64. Mahy, J.G.; Tilkin, R.G.; Douven, S.; Lambert, S.D. TiO2 nanocrystallites photocatalysts modified with metallic species: Comparison between Cu and Pt doping. *Surf. Interfaces* **2019**, *17*, 100366, doi:10.1016/j.surfin.2019.100366.
65. Mahy, J.G.; Lambert, S.D.; Tilkin, R.G.; Wolfs, C.; Poelman, D.; Devred, F.; Gaigneaux, E.M.; Douven, S. Ambient temperature ZrO2-doped TiO2 crystalline photocatalysts: Highly efficient powders and films for water depollution. *Mater. Today Energy* **2019**, *13*, 312–322, doi:10.1016/j.mtener.2019.06.010.
66. Malengreaux, C.M.; Pirard, S.L.; Léonard, G.; Mahy, J.G.; Herlitschke, M.; Klobes, B.; Hermann, R.; Heinrichs, B.; Bartlett, J.R. Study of the photocatalytic activity of Fe3+, Cr3+, La3+ and Eu3+ single-doped and co-doped TiO2 catalysts produced by aqueous sol-gel processing. *J. Alloys Compd.* **2017**, *691*, 726–738, doi:10.1016/j.jallcom.2016.08.211.
67. Maver, K.; Štangar, U.L.; Černigoj, U.; Gross, S.; Korošec, R.C. Low-temperature synthesis and characterization of TiO2 and TiO2–ZrO2 photocatalytically active thin films. *Photochem. Photobiol. Sci.* **2009**, *8*, 657–662, doi:10.1039/b817475j.
68. Mohammadi, M.; Fray, D.; Mohammadi, A. Sol–gel nanostructured titanium dioxide: Controlling the crystal structure, crystallite size, phase transformation, packing and ordering. *Microporous Mesoporous Mater.* **2008**, *112*, 392–402, doi:10.1016/j.micromeso.2007.10.015.
69. Mohammadi, M.R.; Cordero-Cabrera, M.C.; Ghorbani, M.; Fray, D.J. Synthesis of high surface area nanocrystalline anatase-TiO2 powders derived from particulate sol-gel route by tailoring processing parameters. *J. Sol Gel Sci. Technol.* **2006**, *40*, 15–23, doi:10.1007/s10971-006-8267-0.
70. Mutuma, B.K.; Shao, G.; Kim, W.D.; Kim, H.T. Sol–gel synthesis of mesoporous anatase–brookite and anatase–brookite–rutile TiO2 nanoparticles and their photocatalytic properties. *J. Colloid Interface Sci.* **2015**, *442*, 1–7, doi:10.1016/j.jcis.2014.11.060.

71. Okunaka, S.; Tokudome, H.; Hitomi, Y.; Abe, R. Facile preparation of stable aqueous titania sols for fabrication of highly active TiO 2 photocatalyst films. *J. Mater. Chem. A* **2014**, *3*, 1688–1695, doi:10.1039/C4TA04680C.
72. Papiya, F.; Pattanayak, P.; Kumar, V.; Das, S.; Kundu, P.P. Sulfonated graphene oxide and titanium dioxide coated with nanostructured polyaniline nanocomposites as an efficient cathode catalyst in microbial fuel cells. *Mater. Sci. Eng. C* **2020**, *108*, 110498, doi:10.1016/j.msec.2019.110498.
73. Periyat, P.; Saeed, P.; Ullattil, S. Anatase titania nanorods by pseudo-inorganic templating. *Mater. Sci. Semicond. Process.* **2015**, *31*, 658–665, doi:10.1016/j.mssp.2014.12.040.
74. Qi, K.; Xin, J.H. Room-Temperature Synthesis of Single-Phase Anatase TiO2 by Aging and its Self-Cleaning Properties. *ACS Appl. Mater. Interfaces* **2010**, *2*, 3479–3485, doi:10.1021/am1005892.
75. Qiu, X.; Zhao, Y.; Burda, C. Synthesis and Characterization of Nitrogen-Doped Group IVB Visible-Light-Photoactive Metal Oxide Nanoparticles. *Adv. Mater.* **2007**, *19*, 3995–3999, doi:10.1002/adma.200700511.
76. Quintero, Y.; Mosquera, E.; Diosa, J.; García, A. Ultrasonic-assisted sol–gel synthesis of TiO2 nanostructures: Influence of synthesis parameters on morphology, crystallinity, and photocatalytic performance. *J. Sol Gel Sci. Technol.* **2020**, *94*, 477–485, doi:10.1007/s10971-020-05263-6.
77. Ropero-Vega, J.L.; Candal, R.J.; Pedraza-Avella, J.A.; Niño-Gómez, M.E.; Bilmes, S.A. Enhanced visible light photoelectrochemical performance of β-Bi2O3-TiO2/ITO thin films prepared by aqueous sol-gel. *J. Solid State Electrochem.* **2019**, *23*, 1757–1765, doi:10.1007/s10008-019-04270-0.
78. Ryu, D.H.; Kim, S.C.; Koo, S.M.; Kim, D.P. Deposition of Titania Nanoparticles on Spherical Silica. *J. Sol Gel Sci. Technol.* **2003**, *26*, 489–493, doi:10.1023/a:1020791130557.
79. Salahuddin, N.; Abdelwahab, M.; Gaber, M.; Elneanaey, S. Synthesis and Design of Norfloxacin drug delivery system based on PLA/TiO2 nanocomposites: Antibacterial and antitumor activities. *Mater. Sci. Eng. C* **2020**, *108*, 110337, doi:10.1016/j.msec.2019.110337.
80. Ghamsari, M.S.; Radiman, S.; Hamid, M.A.A.; Mahshid, S.; Rahmani, S. Room temperature synthesis of highly crystalline TiO2 nanoparticles. *Mater. Lett.* **2013**, *92*, 287–290, doi:10.1016/j.matlet.2012.10.032.
81. Shinozaki, K.; Zack, J.W.; Richards, R.M.; Pivovar, B.S.; Kocha, S.S. Oxygen Reduction Reaction Measurements on Platinum Electrocatalysts Utilizing Rotating Disk Electrode Technique. *J. Electrochem. Soc.* **2015**, *162*, F1144–F1158, doi:10.1149/2.1071509jes.
82. Shin, H.; Jung, H.S.; Hong, K.S.; Lee, J.-K. Crystallization Process of TiO2Nanoparticles in an Acidic Solution. *Chem. Lett.* **2004**, *33*, 1382–1383, doi:10.1246/cl.2004.1382.
83. Sugimoto, T.; Zhou, X.; Muramatsu, A. Synthesis of uniform anatase TiO2 nanoparticles by gel–sol method 4. Shape control. *J. Colloid Interface Sci.* **2003**, *259*, 53–61, doi:10.1016/s0021-9797(03)00035-3.
84. Sung-Suh, H.M.; Choi, J.R.; Hah, H.J.; Koo, S.M.; Bae, Y.C. Comparison of Ag deposition effects on the photocatalytic activity of nanoparticulate TiO2 under visible and UV light irradiation. *J. Photochem. Photobiol. A Chem.* **2004**, *163*, 37–44, doi:10.1016/s1010-6030(03)00428-3.
85. Tobaldi, D.M.; Pullar, R.; Binions, R.; Jorge, A.B.; McMillan, P.F.; Saeli, M.; Seabra, M.P.; Labrincha, J.A. Influence of sol counterions on the visible light induced photocatalytic behaviour of TiO2 nanoparticles. *Catal. Sci. Technol.* **2014**, *4*, 2134–2146, doi:10.1039/c4cy00423j.
86. Uchiyama, H.; Bando, T.; Kozuka, H. Effect of the amount of H2O and HNO3 in Ti(OC3H7)4 solutions on the crystallization of sol-gel-derived TiO2 films. *Thin Solid Film* **2019**, *669*, 157–161, doi:10.1016/j.tsf.2018.10.050.
87. Vinogradov, A.V.; Vinogradov, V.V. Effect of Acidic Peptization on Formation of Highly Photoactive TiO2 Films Prepared without Heat Treatment. *J. Am. Ceram. Soc.* **2014**, *97*, 290–294, doi:10.1111/jace.12560.
88. Xu, Q.; Anderson, M.A. Synthesis of porosity controlled ceramic membranes. *J. Mater. Res.* **1991**, *6*, 1073–1081, doi:10.1557/jmr.1991.1073.
89. Yamazaki, S.; Fujinaga, N.; Araki, K. Effect of sulfate ions for sol–gel synthesis of Titania photocatalyst. *Appl. Catal. A Gen.* **2001**, *210*, 97–102, doi:10.1016/s0926-860x(00)00797-3.
90. Yang, J.; Mei, S.; Ferreira, J.M.; Norby, P.; Quaresmâ, S. Fabrication of rutile rod-like particle by hydrothermal method: An insight into HNO3 peptization. *J. Colloid Interface Sci.* **2005**, *283*, 102–106, doi:10.1016/j.jcis.2004.08.109.
91. Yu, J.; Leung, M.K.-P.; Ho, W.; Cheng, B.; Zhao, X. Effects of acidic and basic hydrolysis catalysts on the photocatalytic activity and microstructures of bimodal mesoporous Titania. *J. Catal.* **2003**, *220*, 69–78, doi:10.1016/s0021-9517(03)00034-4.
92. Yun, Y.J.; Chung, J.S.; Kim, S.; Hahn, S.H.; Kim, E.J. Low-temperature coating of sol–gel anatase thin films. *Mater. Lett.* **2004**, *58*, 3703–3706, doi:10.1016/j.matlet.2004.07.018.
93. Borlaf, M.; Poveda, J.M.; Moreno, R.; Colomer, M.T. Synthesis and characterization of TiO2/Rh3+ nanoparticulate sols, xerogels and cryogels for photocatalytic applications. *J. Sol Gel Sci. Technol.* **2012**, *63*, 408–415, doi:10.1007/s10971-012-2802-y.
94. Bugakova, D.; Slabov, V.; Sergeeva, E.; Zhukov, M.; Vinogradov, A. Comprehensive characterization of TiO2 inks and their application for inkjet printing of microstructures. *Colloids Surf. A Physicochem. Eng. Asp.* **2020**, *586*, 124146, doi:10.1016/j.colsurfa.2019.124146.
95. Chen, X.; Lou, Y.; Samia, A.C.S.; Burda, C.; Gole, J.L. Formation of Oxynitride as the Photocatalytic Enhancing Site in Nitrogen-Doped Titania Nanocatalysts: Comparison to a Commercial Nanopowder. *Adv. Funct. Mater.* **2005**, *15*, 41–49, doi:10.1002/adfm.200400184.

96. Vorkapic, D.; Matsoukas, T. Effect of Temperature and Alcohols in the Preparation of Titania Nanoparticles from Alkoxides. *J. Am. Ceram. Soc.* **2005**, *81*, 2815–2820, doi:10.1111/j.1151-2916.1998.tb02701.x.
97. Hu, Y.; Yuan, C. Low-temperature preparation of photocatalytic TiO2 thin films from anatase sols. *J. Cryst. Growth* **2005**, *274*, 563–568, doi:10.1016/j.jcrysgro.2004.10.146.
98. Su, C.; Hong, B.-Y.; Tseng, C.-M. Sol–gel preparation and photocatalysis of titanium dioxide. *Catal. Today* **2004**, *96*, 119–126, doi:10.1016/j.cattod.2004.06.132.
99. Wang, J.; Zhao, H.; Liu, X.; Li, X.; Xu, P.; Han, X. Formation of Ag nanoparticles on water-soluble anatase TiO2 clusters and the activation of photocatalysis. *Catal. Commun.* **2009**, *10*, 1052–1056, doi:10.1016/j.catcom.2008.12.060.
100. Wang, J.; Han, X.; Liu, C.; Zhang, W.; Cai, R.; Liu, Z. Adjusting the Crystal Phase and Morphology of Titania via a Soft Chemical Process. *Cryst. Growth Des.* **2010**, *10*, 2185–2191, doi:10.1021/cg901429u.
101. Yang, J.; Mei, S.; Ferreira, J.M. In situ preparation of weakly flocculated aqueous anatase suspensions by a hydrothermal technique. *J. Colloid Interface Sci.* **2003**, *260*, 82–88, doi:10.1016/s0021-9797(02)00190-x.
102. Yang, J.; Mei, S.; Ferreira, J.M.F. Hydrothermal Synthesis of Nanosized Titania Powders: Influence of Peptization and Peptizing Agents on the Crystalline Phases and Phase Transitions. *J. Am. Ceram. Soc.* **2000**, *83*, 1361–1368, doi:10.1111/j.1151-2916.2000.tb01394.x.
103. Yang, J.; Mei, S.; Ferreira, J.M.F. Hydrothermal Synthesis of Nanosized Titania Powders: Influence of Tetraalkyl Ammonium Hydroxides on Particle Characteristics. *J. Am. Ceram. Soc.* **2004**, *84*, 1696–1702, doi:10.1111/j.1151-2916.2001.tb00901.x.
104. Cassaignon, S.; Koelsch, M.; Jolivet, J.-P. From TiCl3 to TiO2 nanoparticles (anatase, brookite and rutile): Thermohydrolysis and oxidation in aqueous medium. *J. Phys. Chem. Solids* **2007**, *68*, 695–700, doi:10.1016/j.jpcs.2007.02.020.
105. Molea, A.; Popescu, V.; Rowson, N.; Dinescu, A.M. Influence of pH on the formulation of TiO2 nano-crystalline powders with high photocatalytic activity. *Powder Technol.* **2014**, *253*, 22–28, doi:10.1016/j.powtec.2013.10.040.
106. Bazrafshan, H.; Tesieh, Z.A.; Dabirnia, S.; Naderifar, A. Low Temperature Synthesis of TiO 2 Nanoparticles with High Photocatalytic Activity and Photoelectrochemical Properties through Sol-Gel Method. *Mater. Manuf. Process.* **2015**, *31*, 119–125, doi:10.1080/10426914.2015.1037899.
107. Kanna, M.; Wongnawa, S. Mixed amorphous and nanocrystalline TiO2 powders prepared by sol–gel method: Characterization and photocatalytic study. *Mater. Chem. Phys.* **2008**, *110*, 166–175, doi:10.1016/j.matchemphys.2008.01.037.
108. Lee, J.H.; Yang, Y.S. Effect of HCl concentration and reaction time on the change in the crystalline state of TiO2 prepared from aqueous TiCl4 solution by precipitation. *J. Eur. Ceram. Soc.* **2005**, *25*, 3573–3578, doi:10.1016/j.jeurceramsoc.2004.09.024.
109. Xie, Y.; Yuan, C. Visible-light responsive cerium ion modified Titania sol and nanocrystallites for X-3B dye photodegradation. *Appl. Catal. B Environ.* **2003**, *46*, 251–259, doi:10.1016/s0926-3373(03)00211-x.
110. Xie, Y.; Yuan, C.; Li, X. Photocatalytic degradation of X-3B dye by visible light using lanthanide ion modified titanium dioxide hydrosol system. *Colloids Surf. A Physicochem. Eng. Asp.* **2005**, *252*, 87–94, doi:10.1016/j.colsurfa.2004.10.061.
111. Xie, Y.; Yuan, C. Photocatalytic and photoelectrochemical performance of crystallized titanium dioxide sol with neodymium ion modification. *J. Chem. Technol. Biotechnol.* **2005**, *80*, 954–963, doi:10.1002/jctb.1270.
112. Zeng, T.; Qiu, Y.; Chen, L.; Song, X. Microstructure and phase evolution of TiO2 precursors prepared by peptization-hydrolysis method using polycarboxylic acid as peptizing agent. *Mater. Chem. Phys.* **1998**, *56*, 163–170, doi:10.1016/s0254-0584(98)00170-9.
113. Zhang, Q.-H.; Gao, L.; Guo, J.-K. Preparation and characterization of nanosized TiO2 powders from aqueous TiCl4 solution. *Nanostruct. Mater.* **1999**, *11*, 1293–1300, doi:10.1016/s0965-9773(99)00421-3.
114. Kattoor, V.; Smitha, V.S.; Mohamed, A.P.; Hareesh, U.N.S.; Warrier, K.G. Temperature assisted acid catalyzed peptization of TiO2; facile sol–gel approach for thermally stable anatase phase. *RSC Adv.* **2014**, *4*, 21664–21671, doi:10.1039/c4ra01939c.
115. Li, Y.; Qin, Z.; Guo, H.; Yang, H.; Zhang, G.; Ji, S.; Zeng, T. Low-Temperature Synthesis of Anatase TiO2 Nanoparticles with Tunable Surface Charges for Enhancing Photocatalytic Activity. *PLoS ONE* **2014**, *9*, e114638, doi:10.1371/journal.pone.0114638.
116. Liu, W.-X.; Jiang, P.; Shao, W.-N.; Zhang, J.; Cao, W.-B. A novel approach for the synthesis of visible-light-active nanocrystalline N-doped TiO2 photocatalytic hydrosol. *Solid State Sci.* **2014**, *33*, 45–48, doi:10.1016/j.solidstatesciences.2014.04.012.
117. Ma, Y.; Zhang, J.; Tian, B.; Chen, F.; Bao, S.; Anpo, M. Synthesis of visible light-driven Eu, N co-doped TiO2 and the mechanism of the degradation of salicylic acid. *Res. Chem. Intermed.* **2012**, *38*, 1947–1960, doi:10.1007/s11164-012-0516-y.
118. Kim, Y.T.; Park, Y.S.; Myung, H.; Chae, H.K. A chelate-assisted route to anatase TiO2 nanoparticles in acidic aqueous media. *Colloids Surf. A Physicochem. Eng. Asp.* **2008**, *313-314*, 260–263, doi:10.1016/j.colsurfa.2007.04.106.
119. Liu, T.-X.; Li, F.-B.; Li, X.-Z. Effects of peptizing conditions on nanometer properties and photocatalytic activity of TiO2 hydrosols prepared by H2TiO3. *J. Hazard. Mater.* **2008**, *155*, 90–99, doi:10.1016/j.jhazmat.2007.11.034.
120. Liu, T.-X.; Li, X.-Z.; Li, F.-B. Enhanced photocatalytic activity of Ce3+-TiO2 hydrosols in aqueous and gaseous phases. *Chem. Eng. J.* **2010**, *157*, 475–482, doi:10.1016/j.cej.2009.12.010.
121. Šuligoj, A.; Štangar, U.L.; Ristić, A.; Mazaj, M.; Verhovšek, D.; Tušar, N.N. TiO2–SiO2 films from organic-free colloidal TiO2 anatase nanoparticles as photocatalyst for removal of volatile organic compounds from indoor air. *Appl. Catal. B Environ.* **2016**, *184*, 119–131, doi:10.1016/j.apcatb.2015.11.007.
122. Zhang, R.; Gao, L. Effect of peptization on phase transformation of TiO2 nanoparticles. *Mater. Res. Bull.* **2001**, *36*, 1957–1965, doi:10.1016/s0025-5408(01)00674-2.
123. Alcober, C.; Alvarez, F.; Bilmes, S.A.; Candal, R.J. Photochromic W-TiO2 membranes. *J. Mater. Sci. Lett.* **2002**, *21*, 501–504.
124. Belet, A.; Wolfs, C.; Mahy, J.G.; Poelman, D.; Vreuls, C.; Gillard, N.; Lambert, S.D. Sol-gel Syntheses of Photocatalysts for the Removal of Pharmaceutical Products in Water. *Nanomaterials* **2019**, *9*, 126, doi:10.3390/nano9010126.

125. Bergamonti, L.; Alfieri, I.; Lorenzi, A.; Montenero, A.; Predieri, G.; Di Maggio, R.; Girardi, F.; Lazzarini, L.; Lottici, P.P. Characterization and photocatalytic activity of TiO2 by sol–gel in acid and basic environments. *J. Sol Gel Sci. Technol.* **2014**, *73*, 91–102, doi:10.1007/s10971-014-3498-y.
126. Borlaf, M.; Moreno, R.; Ortiz, A.L.; Colomer, M.T. Synthesis and photocatalytic activity of Eu3+-doped nanoparticulate TiO2 sols and thermal stability of the resulting xerogels. *Mater. Chem. Phys.* **2014**, *144*, 8–16, doi:10.1016/j.matchemphys.2013.11.058.
127. Hu, L.; Wang, J.; Zhang, J.; Zhang, Q.; Liu, Z. An N-doped anatase/rutile TiO2hybrid from low-temperature direct nitridization: Enhanced photoactivity under UV-/visible-light. *RSC Adv.* **2014**, *4*, 420–427, doi:10.1039/c3ra44421j.
128. Jiang, J.; Long, M.; Wu, D.; Cai, W. Alkoxyl-derived visible light activity of TiO2 synthesized at low temperature. *J. Mol. Catal. A Chem.* **2011**, *335*, 97–104, doi:10.1016/j.molcata.2010.11.019.
129. Khan, H. Sol–gel synthesis of TiO2 from TiOSO4: Characterization and UV photocatalytic activity for the degradation of 4-chlorophenol. *React. Kinet. Mech. Catal.* **2017**, *121*, 811–832, doi:10.1007/s11144-017-1195-x.
130. Mao, L.; Li, Q.; Dang, H.; Zhang, Z. Synthesis of nanocrystalline TiO2 with high photoactivity and large specific surface area by sol–gel method. *Mater. Res. Bull.* **2005**, *40*, 201–208, doi:10.1016/j.materresbull.2004.11.001.
131. Yan, Q.; Wang, J.; Han, X.; Liu, Z. Soft-chemical method for fabrication of SnO–TiO2 nanocomposites with enhanced photocatalytic activity. *J. Mater. Res.* **2013**, *28*, 1862–1869, doi:10.1557/jmr.2013.135.
132. Al-Maliki, F.J.; Al-Lamey, N.H. Synthesis of Tb-doped titanium dioxide nanostructures by sol–gel method for environmental photocatalysis applications. *J. Sol Gel Sci. Technol.* **2016**, *81*, 276–283, doi:10.1007/s10971-016-4190-1.
133. Gole, J.L.; Stout, J.D.; Burda, C.; Lou, Y.; Chen, X. Highly Efficient Formation of Visible Light Tunable TiO $_{2-x}$ N $_{x}$ Photocatalysts and Their Transformation at the Nanoscale. *J. Phys. Chem. B.* **2004**, *108*, 1230–1240.
134. Chung, W.; Kim, S.; Chang, S. A Study of the Correlation Between the Physical Characteristics and Efficiency of TiO2 Photocatalyst Prepared with the Sol–Gel Method. *J. Nanosci. Nanotechnol.* **2016**, *16*, 11040–11045, doi:10.1166/jnn.2016.13286.
135. Huang, Y.; Wang, P.; Wang, Z.; Rao, Y.; Cao, J.-J.; Pu, S.; Ho, W.; Lee, S.-C. Protonated g-C3N4/Ti3+ self-doped TiO2 nanocomposite films: Room-temperature preparation, hydrophilicity, and application for photocatalytic NO removal. *Appl. Catal. B Environ.* **2019**, *240*, 122–131, doi:10.1016/j.apcatb.2018.08.078.
136. Look, J.L.; Zukoski, C.F. Alkoxide-Derived Titania Particles: Use of Electrolytes to Control Size and Agglomeration Levels. *J. Am. Ceram. Soc.* **1992**, *75*, 1587–1595, doi:10.1111/j.1151-2916.1992.tb04230.x.
137. Look, J.-L.; Zukoski, C.F. Colloidal Stability and Titania Precipitate Morphology: Influence of Short-Range Repulsions. *J. Am. Ceram. Soc.* **1995**, *78*, 21–32, doi:10.1111/j.1151-2916.1995.tb08356.x.
138. Sharma, B.; Agarwal, R.; Jassal, M.; Agrawal, A.K. Stabilizer-free low-acid rapid synthesis of highly stable transparent aqueous titania nano sol and its photocatalytic activity. *J. Mol. Liq.* **2020**, *305*, 112842, doi:10.1016/j.molliq.2020.112842.
139. Antonello, A.; Brusatin, G.; Guglielmi, M.; Bello, V.; Mattei, G.; Zacco, G.; Martucci, A. Nanocomposites of titania and hybrid matrix with high refractive index. *J. Nanoparticle Res.* **2011**, *13*, 1697–1708, doi:10.1007/s11051-010-9923-4.
140. Bi-Tao, X.; Bao-Xue, Z.; Long-Hai, L.; Jun, C.; Yan-Biao, L.; Wei-Min, C. Preparation of nanocrystalline anatase TiO2 using basic sol-gel method. *Chem. Pap.* **2008**, *62*, 382–387, doi:10.2478/s11696-008-0040-0.
141. Li, H.; Afanasiev, P. On the selective growth of titania polymorphs in acidic aqueous medium. *Mater. Res. Bull.* **2011**, *46*, 2506–2514, doi:10.1016/j.materresbull.2011.08.023.
142. Mahy, J.G.; Lambert, S.D.; Geens, J.; Daniel, A.; Wicky, D.; Archambeau, C.; Heinrichs, B. Large scale production of photocatalytic TiO2 coating for volatile organic compound (VOC) air remediation. *AIMS Mater. Sci.* **2018**, *5*, 945–956, doi:10.3934/matersci.2018.5.945.
143. Wang, J.-Y.; Yu, J.-X.; Liu, Z.-H.; He, Z.-K.; Cai, R.-X. A simple new way to prepare anatase TiO2 hydrosol with high photocatalytic activity. *Semicond. Sci. Technol.* **2005**, *20*, L36–L39, doi:10.1088/0268-1242/20/8/l03.
144. Nie, X.; Zhuo, S.; Maeng, G.; Sohlberg, K. Doping ofTiO2Polymorphs for Altered Optical and Photocatalytic Properties. *Int. J. Photoenergy* **2009**, *2009*, 294042, doi:10.1155/2009/294042.
145. Xu, Q.; Zhang, J.; Feng, Z.; Ma, Y.; Wang, X.; Li, C. Surface Structural Transformation and the Phase Transition Kinetics of Brookite TiO2. *Chem. Asian J.* **2010**, *5*, 2158–2161, doi:10.1002/asia.201000249.
146. Bakardjieva, S.; Štengl, V.; Szatmary, L.; Subrt, J.; Lukac, J.; Murafa, N.; Niznansky, D.; Cizek, K.; Jirkovsky, J.; Petrova, N. Transformation of brookite-type TiO2 nanocrystals to rutile: Correlation between microstructure and photoactivity. *J. Mater. Chem.* **2006**, *16*, 1709–1716, doi:10.1039/b514632a.
147. Balaganapathi, T.; Kaniamuthan, B.; Vinoth, S.; Arun, T.; Thilakan, P. Controlled synthesis of brookite and combined brookite with rutile phases of titanium di-oxide and its characterization studies. *Ceram. Int.* **2017**, *43*, 2438–2440, doi:10.1016/j.ceramint.2016.11.037.
148. Li, J.-G.; Ishigaki, T. Brookite rutile phase transformation of TiO2 studied with monodispersed particles. *Acta Mater.* **2004**, *52*, 5143–5150, doi:10.1016/j.actamat.2004.07.020.
149. Lin, Y.; Cai, Y.; Qiu, M.; Drioli, E.; Fan, Y. Environment-benign preparation of Ag toughening TiO2/Ti tight ultrafiltration membrane via aqueous sol–gel route. *J. Mater. Sci.* **2015**, *50*, 5307–5317, doi:10.1007/s10853-015-9078-x.
150. Fallet, M.; Permpoon, S.; Deschanvres, J.-L.; Langlet, M. Influence of physico-structural properties on the photocatalytic activity of sol-gel derived TiO2 thin films. *J. Mater. Sci.* **2006**, *41*, 2915–2927, doi:10.1007/s10853-006-5077-2.
151. Mamadou, S.D.; Neil, A.F.; Myung, S.J. Nanotechnology for Sustainable Development. *Nanotechnol. Sustain. Dev.* **2014**, *14*, 101–111, doi:10.1007/978-3-319-05041-6.

152. Sugimoto, T.; Zhou, X.; Muramatsu, A. Synthesis of uniform anatase TiO2 nanoparticles by gel–sol method 3. Formation process and size control. *J. Colloid Interface Sci.* **2003**, *259*, 43–52, doi:10.1016/s0021-9797(03)00036-5.
153. Chang, C.-J.; Lin, C.-Y.; Hsu, M.-H. Enhanced photocatalytic activity of Ce-doped ZnO nanorods under UV and visible light. *J. Taiwan Inst. Chem. Eng.* **2014**, *45*, 1954–1963, doi:10.1016/j.jtice.2014.03.008.
154. Vaiano, V.; Lara, M.; Iervolino, G.; Matarangolo, M.; Navio, J.; Hidalgo, M.C. Photocatalytic H2 production from glycerol aqueous solutions over fluorinated Pt-TiO2 with high {001} facet exposure. *J. Photochem. Photobiol. A Chem.* **2018**, *365*, 52–59, doi:10.1016/j.jphotochem.2018.07.032.
155. Cao, D.; Wang, Y.; Zhao, X. Combination of photocatalytic and electrochemical degradation of organic pollutants from water. *Curr. Opin. Green Sustain. Chem.* **2017**, *6*, 78–84, doi:10.1016/j.cogsc.2017.05.007.